AD

TECHNICAL REPORT ARCCB-TR-95025

EFFECTS OF ION IMPLANTATION ON ELECTROPLATED CHROMIUM

KATHRYN E. NOLL

APRIL 1995

US ARMY ARMAMENT RESEARCH,
DEVELOPMENT AND ENGINEERING CENTER
CLOSE COMBAT ARMAMENTS CENTER
BENÉT LABORATORIES
WATERVLIET, N.Y. 12189-4050

DISCLAIMER

The findings in this report are not to be construed as an official Department of the Army position unless so designated by other authorized documents.

The use of trade name(s) and/or manufacturer(s) does not constitute an official indorsement or approval.

DESTRUCTION NOTICE

For classified documents, follow the procedures in DoD 5200.22-M, Industrial Security Manual, Section II-19 or DoD 5200.1-R, Information Security Program Regulation, Chapter IX.

For unclassified, limited documents, destroy by any method that will prevent disclosure of contents or reconstruction of the document.

For unclassified, unlimited documents, destroy when the report is no longer needed. Do not return it to the originator.

REPORT DOCUMENTATION PAGE

Form Approved
OMB No. 0704-0188

1. AGENCY USE ONLY *(Leave blank)*	2. REPORT DATE	3. REPORT TYPE AND DATES COVERED
	April 1995	Final

4. TITLE AND SUBTITLE
EFFECTS OF ION IMPLANTATION ON ELECTROPLATED CHROMIUM

5. FUNDING NUMBERS
AMCMS No. 6126.24.H180.0
PRON No. 470TEV64471A

6. AUTHOR(S)
Kathryn E. Noll

7. PERFORMING ORGANIZATION NAME(S) AND ADDRESS(ES)
U.S. Army ARDEC
Benet Laboratories, AMSTA-AR-CCB-O
Watervliet, NY 12189-4050

8. PERFORMING ORGANIZATION REPORT NUMBER
ARCCB-TR-95025

9. SPONSORING / MONITORING AGENCY NAME(S) AND ADDRESS(ES)
U.S. Army ARDEC
Close Combat Armaments Center
Picatinny Arsenal, NJ 07806-5000

10. SPONSORING / MONITORING AGENCY REPORT NUMBER

11. SUPPLEMENTARY NOTES

12a. DISTRIBUTION / AVAILABILITY STATEMENT
Approved for public release; distribution unlimited.

12b. DISTRIBUTION CODE

13. ABSTRACT *(Maximum 200 words)*

In this report, the effects of ion implantation on two kinds of electroplated chromium have been studied. Both hard chromium and low contraction chromium were plated onto samples of 4340 grade steel and subsequently implanted with N_2^+ or Ar^+ at atom energies of 75 keV. The dose was varied from 9.4×10^{15} to 3.1×10^{18} atoms/cm^2 and the implantations were conducted at both room temperature and 500°C. SIMS and AES analyses, Knoop microhardness, and pin-on-disk wear testing were used to study the effects of ion implantation on the surface properties of the chromium plating.

The greatest improvement in the properties was observed for the nitrogen implantations. In general, the hardness, wear, and friction properties improved with an increasing nitrogen dose. For both kinds of chromium, the nitrogen implantation resulted in a 50% reduction in the coefficient of friction and a measurable decrease in the wear rate. At the intermediate doses tested, some of the samples implanted with nitrogen at elevated temperature showed improved friction and wear properties compared to the room temperature samples implanted at the same condition. The elevated temperature implantations also appeared to decrease the hardness of the bulk chromium. For the room temperature, nitrogen implantations, the hardness was increased three times that of the unimplanted hard chromium and slightly less than twice that of the unimplanted low contraction chromium. At the highest dose tested, the maximum nitrogen concentration reached approximately 40 at% for both the room and elevated temperature conditions.

14. SUBJECT TERMS
Ion Implantation, Chromium, Electroplating, Material Properties, Nitrogen, Friction, Wear Properties

15. NUMBER OF PAGES
75

16. PRICE CODE

17. SECURITY CLASSIFICATION OF REPORT	18. SECURITY CLASSIFICATION OF THIS PAGE	19. SECURITY CLASSIFICATION OF ABSTRACT	20. LIMITATION OF ABSTRACT
UNCLASSIFIED	UNCLASSIFIED	UNCLASSIFIED	UL

GENERAL INSTRUCTIONS FOR COMPLETING SF 298

The Report Documentation Page (RDP) is used in announcing and cataloging reports. It is important that this information be consistent with the rest of the report, particularly the cover and title page. Instructions for filling in each block of the form follow. It is important to ***stay within the lines*** to meet ***optical scanning requirements***.

Block 1. Agency Use Only *(Leave blank)*.

Block 2. Report Date. Full publication date including day, month, and year, if available (e.g. 1 Jan 88). Must cite at least the year.

Block 3. Type of Report and Dates Covered. State whether report is interim, final, etc. If applicable, enter inclusive report dates (e.g. 10 Jun 87 - 30 Jun 88).

Block 4. Title and Subtitle. A title is taken from the part of the report that provides the most meaningful and complete information. When a report is prepared in more than one volume, repeat the primary title, add volume number, and include subtitle for the specific volume. On classified documents enter the title classification in parentheses.

Block 5. Funding Numbers. To include contract and grant numbers; may include program element number(s), project number(s), task number(s), and work unit number(s). Use the following labels:

C	- Contract	**PR**	- Project
G	- Grant	**TA**	- Task
PE	- Program Element	**WU**	- Work Unit Accession No.

Block 6. Author(s). Name(s) of person(s) responsible for writing the report, performing the research, or credited with the content of the report. If editor or compiler, this should follow the name(s).

Block 7. Performing Organization Name(s) and Address(es). Self-explanatory.

Block 8. Performing Organization Report Number. Enter the unique alphanumeric report number(s) assigned by the organization performing the report.

Block 9. Sponsoring/Monitoring Agency Name(s) and Address(es). Self-explanatory.

Block 10. Sponsoring/Monitoring Agency Report Number. *(If known)*

Block 11. Supplementary Notes. Enter information not included elsewhere such as: Prepared in cooperation with...; Trans. of...; To be published in.... When a report is revised, include a statement whether the new report supersedes or supplements the older report.

Block 12a. Distribution/Availability Statement. Denotes public availability or limitations. Cite any availability to the public. Enter additional limitations or special markings in all capitals (e.g. NOFORN, REL, ITAR).

- **DOD** - See DoDD 5230.24, "Distribution Statements on Technical Documents."
- **DOE** - See authorities.
- **NASA** - See Handbook NHB 2200.2.
- **NTIS** - Leave blank.

Block 12b. Distribution Code.

- **DOD** - Leave blank.
- **DOE** - Enter DOE distribution categories from the Standard Distribution for Unclassified Scientific and Technical Reports.
- **NASA** - Leave blank.
- **NTIS** - Leave blank.

Block 13. Abstract. Include a brief *(Maximum 200 words)* factual summary of the most significant information contained in the report.

Block 14. Subject Terms. Keywords or phrases identifying major subjects in the report.

Block 15. Number of Pages. Enter the total number of pages.

Block 16. Price Code. Enter appropriate price code *(NTIS only)*.

Blocks 17. - 19. Security Classifications. Self-explanatory. Enter U.S. Security Classification in accordance with U.S. Security Regulations (i.e., UNCLASSIFIED). If form contains classified information, stamp classification on the top and bottom of the page.

Block 20. Limitation of Abstract. This block must be completed to assign a limitation to the abstract. Enter either UL (unlimited) or SAR (same as report). An entry in this block is necessary if the abstract is to be limited. If blank, the abstract is assumed to be unlimited.

★U.S.GPO:1991-0-293-947

EFFECTS OF ION IMPLANTATION ON ELECTROPLATED CHROMIUM

CONTENTS

LIST OF TABLES

LIST OF FIGURES

ABSTRACT

In this report, the effects of ion implantation on two kinds of electroplated chromium have been studied. Both hard chromium and low contraction chromium were plated onto samples of 4340 grade steel and subsequently implanted with N_2^+ or Ar^+ at atom energies of 75 keV. The dose was varied from 9.4×10^{15} to 3.1×10^{18} atoms/cm^2 and the implantations were conducted at both room temperature and 500°C. SIMS and AES analyses, Knoop microhardness, and pin-on-disk wear testing were used to study the effects of ion implantation on the surface properties of the chromium plating.

The greatest improvement in the properties was observed for the nitrogen implantations. In general, the hardness, wear, and friction properties improved with an increasing nitrogen dose. For both kinds of chromium, the nitrogen implantation resulted in a 50% reduction in the coefficient of friction and a measurable decrease in the wear rate. At the intermediate doses tested, some of the samples implanted with nitrogen at elevated temperature showed improved friction and wear properties compared to the room temperature samples implanted at the same condition. The elevated temperature implantations also appeared to decrease the hardness of the bulk chromium. For the room temperature, nitrogen implantations, the hardness was increased three times that of the unimplanted hard chromium and slightly less than twice that of the unimplanted low contraction chromium. At the highest dose tested, the maximum nitrogen concentration reached approximately 40 at% for both the room and elevated temperature conditions.

1. INTRODUCTION AND HISTORICAL REVIEW

Ion implantation is a surface modification technique that has been used in a variety of applications over the past several decades. As early as the 1960's, the electronics industry began using ion implantation to change the electrical properties of semiconductors[1]. In the early 1970's, the Atomic Energy Research Establishment in Harwell, England, headed by G. Dearnaley, explored the use of ion implantation for changing the tribological properties of production tools[2]. Since the 1970's, a significant number of articles, books, and conferences have been entirely devoted to the non-semiconductor applications of ion implantation. These studies have included investigating the wear, friction, hardness, fatigue, corrosion, and oxidation behavior of a variety of materials. Materials such as metals, ceramics, composites, and even plastics have all received recent attention[3-8].

Ion implantation offers some unique properties over other conventional surface treatments such as plating, case hardening, or alloying. Since ion implantation is a non-thermodynamic process, solid-solubility limits in a material can be exceeded. Also, there are no adhesion or delamination problems that are associated with plating because the implanted species become an integral part of the base material. Ion implantation is a low temperature process and therefore, does not change the properties of the bulk material. It also causes no significant dimensional changes in the component. Finally, it is a highly repeatable process and is capable of extremely controllable depth concentrations. The major disadvantages of the technique are that it provides only a shallow penetration into the part, it is a line-of-sight process, and there

are still relatively expensive equipment and processing costs associated with implantation. The development of new equipment and processing techniques is, however, attempting to overcome the limitations of conventional ion implantation.

1.1 Ion Implantation Principles

1.1.1 Process

Ion implantation is the process of modifying the physical or chemical surface properties of a solid material by embedding it with ions of a selected element. This enables the electrical, optical, or mechanical properties of a material to be altered. Ions of almost any element can be injected into the solid to a controlled depth and concentration. The depth of penetration is on the order of tenths of a micron and the dose typically ranges from 10^{11} to 10^{18} ions/cm^2 depending on the application. In the semiconductor industry, only relatively small alloying additions, 10^{11} to 10^{15} ions/cm^2, are needed to change the electrical properties of components. When obtaining tribological improvements, significantly larger ion doses, typically between 10^{15} to 10^{18} ions/cm^2, are required to alter most properties of interest. There are several conditions that effect the ion penetration and concentration including the ion energy (acceleration potential), ion mass, sputtering effects, implantation temperature, and substrate material.

For ion implantation, ion energies in the range of a few keV to a few hundred keV are generally used depending on the implantation system. A typical ion implanter consists of an ion source, a mass separator, an acceleration tube, and a target chamber. The element selected for implantation is first ionized in the ion source. From the

source, ions are extracted by small accelerating voltages and channeled into analyzer magnets. The ions are separated, due to the differences in the mass and charge, and only the selected ions are injected into the main acceleration tube. This insures that only a single ion species is implanted at a time. In the acceleration tube, electric fields propel the selected ions toward the target chamber. While the ions get accelerated to a fixed, desired energy, the ion beam is also focused and shaped. The high energy ions are thus accelerated onto the target and are implanted in the near surface of the material[9].

1.1.2 Energy Mechanisms

When a high energy ion penetrates a solid surface, it undergoes a series of collisions with both target atoms and electrons. In these collisions, the incident ion loses energy at a rate of a few to 100 eV per nanometer depending on a number of parameters including the mass and energy of the ion as well as the target material[10]. The entire collision process is typically completed within 10^{-13} seconds of the initial primary collision[11]. The energy loss mechanisms involve two basic processes, nuclear collisions and electronic interactions.

Nuclear collisions occur when the incoming ion directly impacts the nucleus of a target atom. This type of collision usually results in significant scattering of the incoming ions and the dislocation of target atoms from their equilibrium positions. The target atoms are displaced if the energy transferred exceeds a critical amount called the displacement threshold energy, E_d. The displaced atoms can thus displace other atoms leading to a cascade of atomic collisions. A schematic of the collision

cascade is shown in Figure 1.1. The nuclear collisions lead to disorder or damage in the target material consisting of vacancies, interstitial atoms, amorphous regions, and other types of defects. Nuclear collisions can involve large, discrete energy losses and are the dominant energy loss mechanism at low ion energies and heavier ions[10].

Electronic interactions occur when the incoming ion passes through the electronic cloud of a target atom. Energy is transferred from the incoming ion to the electrons either by exciting or ejecting the electrons from their atomic orbitals. This type of interaction usually results in the negligible scattering of the incident ion, negligible lattice disorder, and a much smaller energy loss per collision. Electronic interactions are the dominant energy loss mechanism at high ion energies and for lighter ions[10].

1.1.3 Ion Range

The ion range, R, is the total distance traveled by the ion in the target material. The mechanisms of energy loss enable us to predict the total path covered by the ion as it is brought to rest from an initial energy E_o. The range is determined by the rate of energy loss and can be written as[9]

$$R(E_o) = \int_0^{E_o} \frac{1}{(-dE/dx)}\, dE \qquad (1.1)$$

where the energy loss, dE/dx, consists of contributions from both the nuclear and electronic collisions. The final resting place of an implanted ion is decided by these energy loss mechanisms as well as the ions possible relocation by subsequent cascades. Because each ion strikes the target with different random impact parameters, not all ions will come to rest at the same depth into the material. The ion

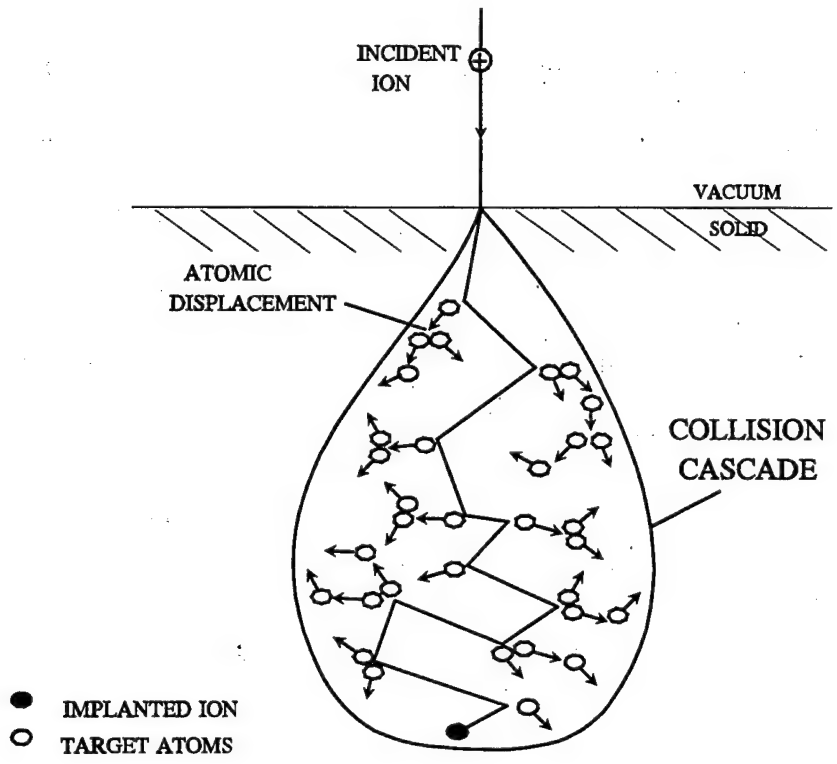

Figure 1.1 Schematic of the collision cascade, the ion-solid interactions, and the ion implantation process.

depth distribution is best approximated by a normal Gaussian curve, with the peak corresponding to the projected ion range. Figure 1.2 schematically shows the ion range R, the projected range R_p, the projected straggle ΔR_p, and the lateral straggle ΔR_L. R_p is the projected distance of travel in the direction of incidence. The projected straggle, ΔR_p, is the standard deviation of the Gaussian distribution in the incoming ion direction, and the lateral straggle, ΔR_L, is perpendicular to the ion direction. The projected range distribution, N(x), can be approximated by the following equation[10]

$$N(x) = N_{(max)} \exp\left[\frac{-1}{2} \left(\frac{x - R_p}{\Delta R_p} \right)^2 \right] \qquad (1.2)$$

where N(x) is the concentration of ions as a function of depth, x, measured in a direction perpendicular to the material surface, and N_{max} is the maximum of the concentration at $x = R_p$. A schematic of the Gaussian distribution is shown in Figure 1.3.

In real life the Gaussian distribution gives only a first-order approximation to the true concentration profile. Actual profiles show an asymmetrical distribution associated with the backscattering of implanting ions by the substrate atoms. Lighter ions will experience backscattering larger than predicted by equation 1.2 and the Gaussian curve will have an asymmetry on the surface side of the maximum. Heavier ions will experience less backscattering and the curve will have a skewness on the deeper side of the maximum[9].

In crystalline materials, the orientation of the ion beam with respect to the

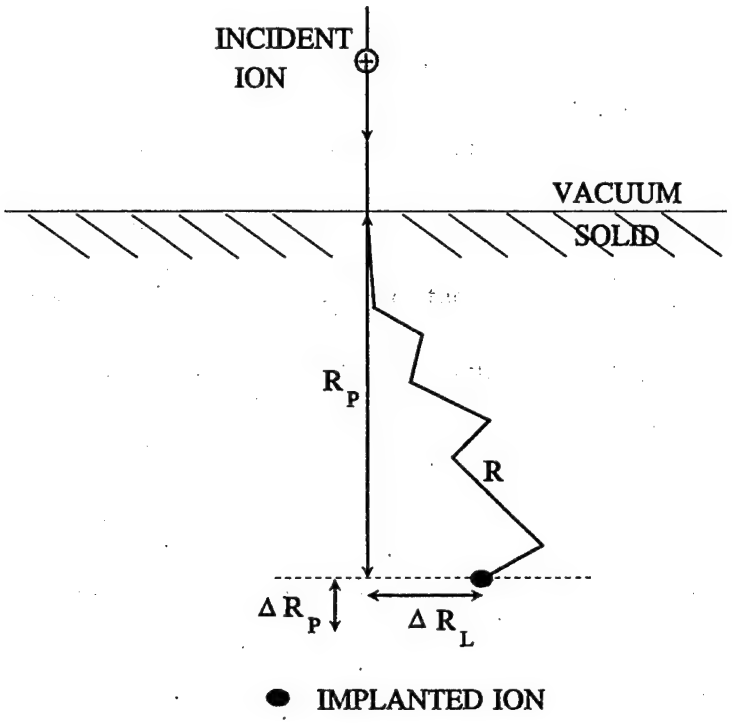

Figure 1.2 Schematic of the ion range R, the projected range R_p, the projected straggle ΔR_p, and the lateral straggle ΔR_L.

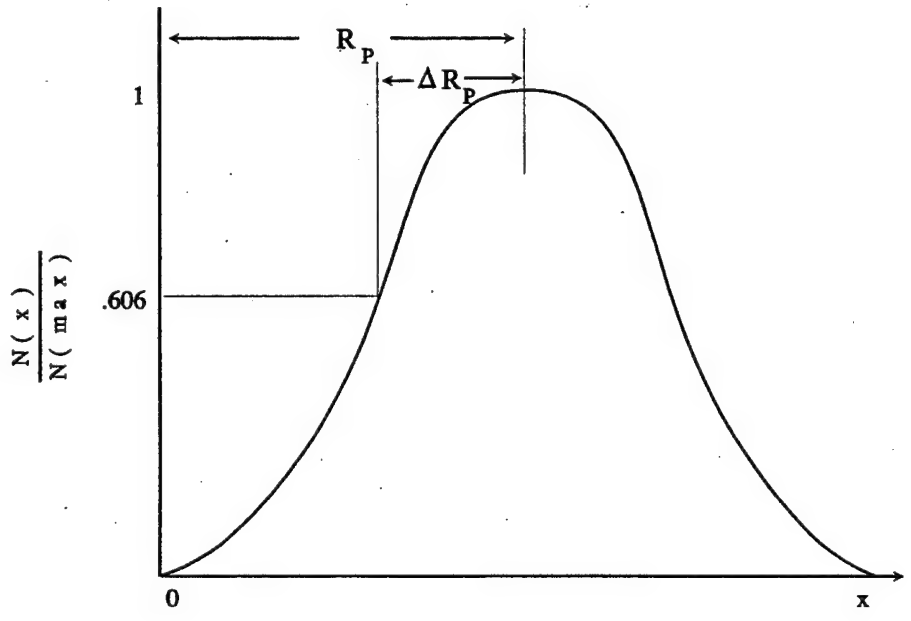

Figure 1.3 One-dimensional Gaussian curve depicting the projected range distribution N(x), the mean value R_p, and a standard deviation ΔR_p, from the mean.

target material can also affect the range distribution. Ion implantation along crystallographic axes can lead to enhanced ion penetration. This phenomenon is known as channeling. The channeled ions have a much lower rate of energy loss and thus a greater range than nonchanneled ions.

The theoretical prediction of the projected ion range distribution has also been approached using computer programs such as transport of ions in matter (TRIM). These programs consider the dynamics of the collision cascade and simulate it as a series of binary elastic collisions based on linear transport theory.

1.1.4 Influences on Material Properties

The changes in a material's properties after ion implantation are the result of several types of effects. One of these is a chemical or alloying effect due to the presence of the implanted ions. The amount of alloying ion implantation can produce in a material is influenced by the ion species, target material, ion dose, and sputtering effects. During high-dose implantation, prolonged irradiation can lead to appreciable surface erosion and ultimately to the removal of already implanted atoms. This sputtering of the surface provides an effective limit to the concentration of implanted ions that can be attained by implantation. For this reason, concentration levels are often measured after implantation to determine the retained ion dose compared to the actual implanted dose.

Temperature is another important influence. According to some research[12,13], temperature effects may influence the mechanical and chemical properties of a material. In some cases, elevated temperature implantation has been shown to increase

the depth of the ion penetration[14] and change the shape of the concentration profile[12]. Other research has shown that with increased temperature, a higher retained ion dose can be attained[13]. These observed effects have been explained, in part, by thermal diffusion. These changes in surface properties may be achieved through elevated temperature implantation or by subsequent annealing after room temperature implantation.

The effect of disorder can also influence a material's properties. In a crystalline material, a disordered region is produced in the surface by the collision cascades. The disorder created can, in some cases, be beneficial and produce desired property changes. For example, diffusion rates may be enhanced and the surface may become more corrosion-resistant[1].

1.2 Ion Implantation Methods

There are several methods in which ions can be implanted into a material. Two of the more common methods used are direct implantation and ion beam mixing. Recently, other methods such as dynamic ion mixing (DIM) and plasma source ion implantation (PSII) have exploited the advantages of ion implantation while attempting to overcome some of its limitations.

1.2.1 Direct Ion Implantation

Direct ion implantation is the process that has been described previously in the last section. A beam of ions is generated by a particle accelerator, propagated and focused along an acceleration tube, and swept or rastered across the target. The ions are thus directly imbedded in the surface of a material.

1.2.2 Ion Mixing

In ion beam mixing, a thin-film layer is deposited on top of a material and bombarded with heavy ions of inert gases. During the process, an intermixing occurs within the collision cascade leading to the formation of a compound at the target/film interface. A schematic of the process is shown in Figure 1.4. The first ion beam mixing experiment was conducted in 1973 and since that time a wide variety of atomic elements have been mixed and new alloys produced[15]. Ion beam mixing offers the advantage of modifying materials with significantly lower ion doses, i.e., 10^{15} ions/cm^2, compared to those required for materials modification by direct implantation. Each ion causes mixing primarily over its range or the dimensions of the collision cascade. The amount of ion beam mixing is directly related to the energy loss per unit distance of the ion travelled. Therefore, the mixing is more effective the higher the dose and the mass of the ions. Ion energy also plays an important role in ion beam mixing. Low energy ions produce mixing near the surface, whereas high energy ions cause the mixing into the interior of the substrate[9]. This method is still limited by the shallow depth of treatment which is on the order of the ion penetration depth, 0.1 to 0.2 μm. The mixing process may involve simple collisional mixing or more complicated beam-induced diffusional processes.

1.2.3 Dynamic Ion Mixing

Dynamic ion mixing combines ion beam mixing with simultaneous film deposition. In the first stage of deposition when the film thickness, t, is less than the projected ion range, R_p, most of the atomic displacements in the collision cascades are

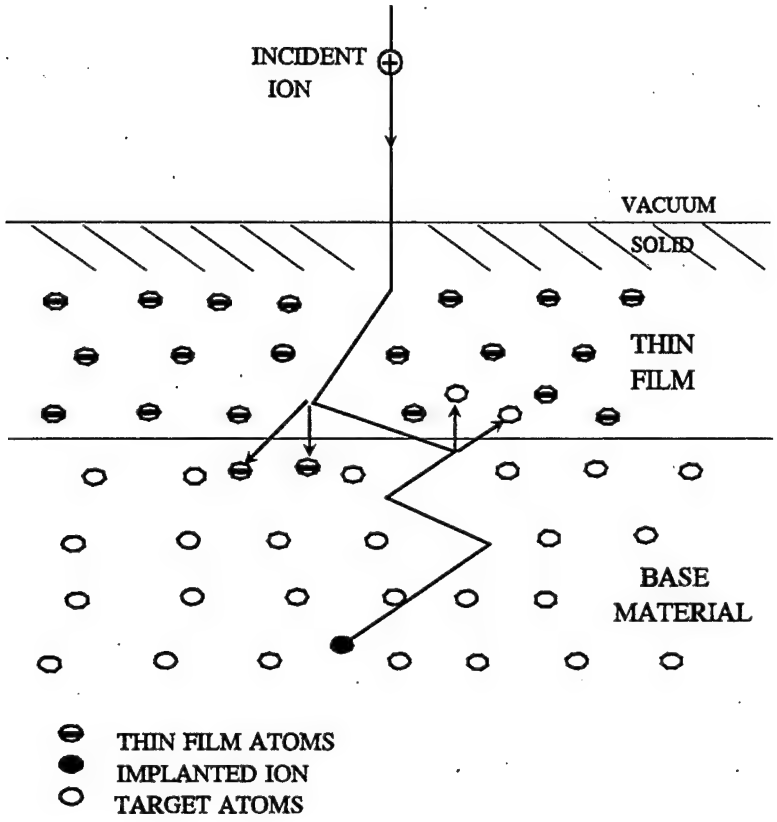

Figure 1.4 Schematic of the ion-beam mixing process.

produced within the target material. When $t \approx R_p$, all the ion energy is then deposited in the coating material. This process results in an intermixed layer at the target/film interface of graded composition, thus greatly improving the adhesion performance of the films. This method also removes some of the thickness limitations of ion beam mixing and allows for the buildup of thicker coatings, 1 to 2 μm, on engineering components. This technique preserves all the advantages of ion implantation, in addition to those of physical vapor deposition (PVD) methods. Some other positive aspects of DIM have been observed, such as the suppression of columnar growth or the modification of the residual stresses stored in a film[15]. The main limitation of the dynamic ion mixing process is its dependence on the deposition rate of the film.

1.2.4 Plasma Source Ion Implantation

Plasma source ion implantation (PSII) is one of the more recent discoveries in the field of ion implantation. The technique was first proposed by Conrad *et al.* at the University of Wisconsin in 1987[16]. The process involves immersing the target into a weakly ionized plasma containing the ions to be implanted. The target is pulsed repeatedly to a high negative potential. During each pulse, the positive ions are accelerated across the plasma sheath toward the target material and implanted in its surface. This method does not have the limitation of being a line-of-sight process. Ions are accelerated perpendicular to the target, so the implant can conform to the shape of the target without masking and manipulating the target or rastering an ion beam. This perpendicular implant maximizes the implant depth and minimizes sputtering. PSII is also considerably faster than traditional techniques because the

high-current, pulsed-power supply provides significantly higher average currents than conventional beam accelerators.

To date, the published results for PSII have been for small objects[16,17], generally no larger than 0.1 m^2. But initial testing of a large-scale PSII facility where surface areas exceeding 1 m^2 at doses of up to 5 x 10^{17} ions/cm^2, has recently been reported[17].

1.3 Current Applications of Ion Implantation

The commercial uses for ion implantation have mostly been in the areas of solid-state electronics, biomedical materials, aerospace and defense materials, and certain production tooling. Ions that are typically used for non-semiconductor commercial applications are N^+, C^+, B^+, Y^+, Ti^+, and Cr^+. Laboratory experiments and industrial trials have confirmed that significant improvements in such properties as wear, friction, hardness, corrosion, oxidation, and fatigue can be obtained by ion implantation in a wide range of materials. A brief description of some of the implantation conditions examined, materials investigated, and results found in these areas will be discussed.

As will be shown, there often appears to be an optimum implantation condition for improving the surface properties of different materials, above or below which properties can actually deteriorate. The difficulty in determining which condition should be used in a particular application is considerable. Therefore, further understanding of the mechanisms behind the various property changes is still needed.

1.3.1 Wear, Friction, and Hardness

Numerous research has been conducted on the tribological behavior of ion implanted materials. Onate *et al.*[18] examined the effects of nitrogen implantation on hard chromium at an ion energy of 90 keV and nitrogen doses in excess of 10^{17} ions/cm^2. The wear resistance was increased to approximately four times that of the unimplanted samples. The surface hardness was also improved by a maximum of 43% at an optimum dose. They found that at higher doses a hardness value lower than the maximum was actually obtained. The coefficient of friction was also reduced at least during the run-in period. Guzman *et al.*[19] found similar hardness results on nitrogen implanted cemented tungsten carbide. The samples were implanted with molecular nitrogen ions, N_2^+, at 90 keV over a range of doses, 3 x 10^{16} to 1 x 10^{18} ions/cm^2, and temperatures, 70 to 550°C. They discovered an increase in surface hardness of up to 40% with an optimum dose between 1 and 3 x 10^{17} ions/cm^2 for the different grades evaluated. They also found that optimum hardness improvements were obtained in the temperature range 140 to 440°C with a distinct softening occurring at 470°C and no improvement at 70°C. Fischer *et al.*[20] observed the effects of nitrogen ion implantation on the tribological properties of metallic surfaces. Three coatings were investigated, electroplated hard chromium, phosphate coating, and plasma face-coated hard molybdenum. The coatings were plated onto grey cast iron and implanted with N_2^+ at ion energies of up to 75 keV and doses up to 10^{18} ions/cm^2. The implantations resulted in up to 31% wear reduction and 7% friction coefficient reduction for the chromium surface, up to 24% wear reduction and 13% friction coefficient reduction

for the phosphate coating, and up to 90% wear reduction and 84% surface hardness increase for the molybdenum deposit.

1.3.2 Corrosion and Oxidation

Stroosnijder *et al.*[21] examined the effect of cerium implantation on the corrosion behavior of wrought austenitic Fe-20Cr-32Ni steel in a hydrogen-based gas mixture at 700°C. The ion energy used was 200 keV and the dose either 10^{16} or 10^{17} ions/cm^2. The gas mixture consisted of 7% CO, 1.2% H_2O, and 0.2% H_2S. The samples were exposed for periods of minutes up to 1000 hours. For the higher-dose implantations, a decrease in the mass gain by a factor of up to three was observed and a clear retardation of the corrosion rate was seen for durations of up to 200 hours.

Kothari *et al.*[22] investigated the effects of N_2^+ ion implantation on the oxidation of polycrystalline copper. 30 keV ions were implanted at doses ranging from 8×10^{15} to 4×10^{17} N atoms/cm^2 with the oxidation carried out at 200 and 600°C. It was determined that at doses from 5×10^{16} to 2×10^{17} N atoms/cm^2 the oxidation resistance of the copper was improved. At doses less than 5×10^{16} N atoms/cm^2 the oxidation properties deteriorated, and at doses higher than 2×10^{17} bubbles formed that were harmful for high-temperature oxidation. Lobb and Bennett[23] studied the oxidation resistance of 20Cr-25Ni-Nb stainless steel in a carbon dioxide-based environment for test durations of 0.5 and 1 hour at 1300°C. The material was implanted with cerium and yttrium at an ion dose of 10^{17} ions/cm^2. The gas mixture consisted of CO_2 + 1% CO. They found that the implantation of either cerium or yttrium ions was effective in reducing oxidation at temperatures $\leq$ 1000°C, but was

totally ineffective at 1300°C.

1.3.3 Fatigue

Hu *et al.* measured fatigue life improvements in AISI 1018 steel[24]. The fatigue test specimens were implanted with N_2^+ ions at an ion energy of 150 keV and a dose of 1 x 10^{17} ions/cm^2. They observed no difference in fatigue life between the implanted and unimplanted samples. But samples implanted and aged for 4 months at room temperature or aged at 100°C for 6 hours, led to a two order-of-magnitude improvement in fatigue life. Lee and Mansur[25] investigated the effect of B^+ and N_2^+ implantation on the fatigue life of Fe-13Cr-15Ni base austenitic alloys. The specimens were implanted with 400 keV B^+, 1.1 MeV N_2^+, or simultaneously with both. The ion dose was 2.3 x 10^{16} ions/cm^2 for most cases. In general, the fatigue life increased in the order of nitrogen, boron, and boron-nitrogen implantation. The nitrogen produced a 33% increase in fatigue life in one of the alloys but caused no change or a decrease in fatigue life in the presence of titanium in other alloys. Boron was very effective in the presence of molybdenum and produced a 99% improvement alone and a 250% improvement when implanted in combination with nitrogen. The simultaneous implantation of B^+ and N_2^+ resulted in the greatest improvement in fatigue life with an increase observed for all the alloys tested.

1.4 Electroplated Chromium

Electroplated chromium has played an important role in the coating industry for a variety of machine tooling, process equipment, and manufactured products. The technology of plating with chromium has been around since the 1920's. It has been

widely used for both decorative and engineering applications. Among the engineering applications are improving corrosion, wear, and erosion resistances, lowering friction coefficients, and increasing the hardness of a component. Chromium plating has also been used to restore the dimensions of undersized parts.

Two kinds of chromium films were investigated in this study, hard chromium and low contraction chromium. Hard chromium coatings are extremely hard and corrosion resistant but are relatively brittle and contain numerous microcracks. They are commonly used as protective coatings to increase the service life of parts by increasing their resistance to wear, abrasion, heat, or corrosion. Applications include automotive valve stems, piston rings, shock rods, the bores of diesel and aircraft cylinders, and hydraulic shafts[26]. Low contraction chromium coatings are much softer but are relatively crack-free and have high strength characteristics. The films also have good lubricity and resistance to shock. Applications for low contraction chromium include broaches, cams, dies for metal forming, and metalworking rolls. Both kinds of chromium films are produced by electrodeposition from a plating solution. The different characteristics of the films are the result of different plating conditions.

In general, chromium coatings are applied to material surfaces to enhance their mechanical, thermal, or chemical properties. As mentioned previously, ion implantation can also offer improvements to materials in these areas. With the ever-increasing demand for enhanced performance of materials, certain applications may benefit from the combined protection of a coating and ion implantation. Therefore, it

is the intention of this study to investigate the effects of ion implantation on electroplated chromium. The dose, ion species, and implantation temperature have been varied and the hardness, wear resistance, friction coefficient, and ion concentration versus depth have been measured.

2. EXPERIMENTAL PROCEDURES

2.1 Sample Preparations

Two different types of samples were prepared for this experiment. Flat disks, 3.81 cm in diameter and 1.27 cm high, were prepared for the wear and friction testing. Flat-headed pins, 1.27 cm long, 6.4 mm in diameter tapering to a 3.2 mm diameter tip, were used for the hardness measurements and secondary ion mass spectrometry (SIMS) analysis. The base material for the samples was made from a heat-treated, high strength steel, AISI 4340 grade. The samples were mechanically polished with a 3 μm diamond spray and then electroplated. The chromium plating solution used consisted of 250 g/ℓ chromic acid and 2.5 g/ℓ sulfuric acid. The hard chromium was deposited using a cathodic current of 30 A/dm^2 at a plating solution temperature of 55°C. The low contraction chromium was deposited using a cathodic current of 120 A/dm^2 at a plating solution temperature of 85°C. The plating time was chosen to produce a film thickness of approximately 75 to 100 μm. The samples were again mechanically polished with a 3 μm diamond spray and their surface roughness was determined using a Wyko optical profilometer. The average surface roughness was around 14 nm R_a or 20 nm RMS. Figure 2.1 shows a representative measurement of a sample. The vertical scale in the figure is given in nanometers and the peak-to-valley measurement, denoted P-V on the figure, is listed in the upper right-hand corner.

2.2 Characterization of As-plated Chromium

Samples of both types of electroplated chromium were cut cross-sectionally and

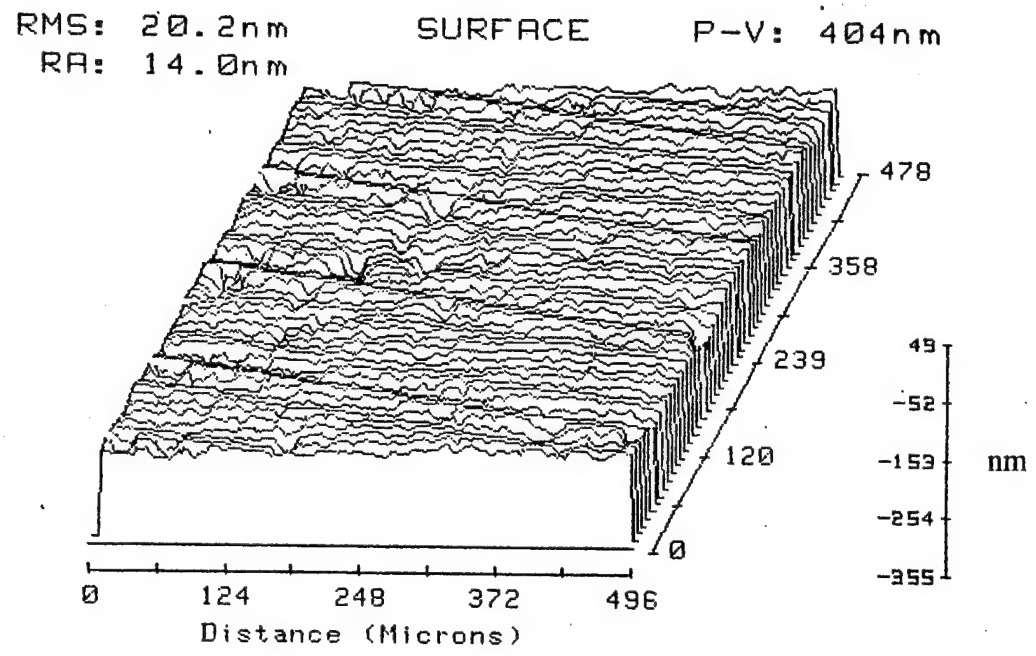

Figure 2.1 Representative surface roughness measurement taken on polished chromium plated samples. The average roughness was approximately 14 nm R_a or 20 nm RMS.

metallographically prepared. Hardness measurements were taken on a cross-section of the plating with a Knoop diamond indenter using a 100-gram load. A chemical analysis was conducted using a Perkin Elmer 6500 Inductively Coupled Plasma (ICP) Spectrometer to verify the composition of the chromium plating. To examine the microstructure, the samples were etched with a 30 mL hydrochloric acid and 10 mL nitric acid solution to reveal the morphology of the plating. The samples were examined in the as-polished and etched conditions using an optical microscope and a scanning electron microscope.

2.3 Ion Implantation Conditions

The hard chromium and low contraction chromium plated samples were subjected to ion implantation using an Extrion Model 400 ion implanter. The nitrogen ion implantation was performed by using an N_2^+ ion beam. For all conditions, the nitrogen implantation was performed at an energy of 150 keV. This represents an individual atomic ion energy of 75 keV. The doses ranged from 9.4×10^{15} to 3.1×10^{18} N atoms/cm^2. A control ion implantation was performed by using an Ar^+ ion beam. For all conditions, the argon implantation was performed at an ion energy of 75 keV. The doses ranged from 9.4×10^{15} to 3.1×10^{17} atoms/cm^2. The implantations were carried out at room temperature and elevated temperatures, at a pressure typically around 10^{-6} torr. During the room temperature implantations, the sample temperature was monitored and did not exceed 180°C. The elevated temperature implants entailed heating the samples to 500°C prior to implantation and maintaining them at that temperature throughout the implant. The sample heating time

was approximately one hour. The average beam current density on the samples was about 3 to 4 $\mu A/cm^2$. Liquid nitrogen traps were used in an attempt to reduce the surface contamination by the vacuum system hydrocarbons.

2.4 SIMS and AES Analyses

Secondary ion mass spectrometry (SIMS) combined with Auger electron spectroscopy (AES) was used to characterize the implantation profiles and chemical composition of the implanted chromium films. Concentration profiles determined from these analyses were compared with the results obtained from TRIM simulations. The SIMS and AES analyses were conducted at Evans East, Plainsboro, NJ, using a Perkin Elmer 6300 SIMS instrument and a Perkin Elmer Model 660 AES instrument. The SIMS profiling was done using a 5.0 keV Cs^+ ion as the primary beam and observing the positive secondary ion yield from the sample as a function of time. The samples were analyzed for nitrogen and argon, but carbon and oxygen were also monitored to determine if there were any substantial amounts of implanted impurities. During implantation, carbon and oxygen surface contamination is usually attributed to the reaction with either residual CO or organic species in the vacuum. For some samples, Auger analysis was used to further quantify the implant concentration. Conversion of nitrogen ion and argon ion counts/second to concentrations/second was accomplished by calculating the relative sensitivity factors using the calculated doses of the implants. Depth scales were determined by measuring the post-bombardment craters using a Dektak stylus profilometer.

2.5 Hardness Measurements

Surface hardness was measured using a Leitz optical microscope with a Knoop diamond indenter. The Knoop microhardness indenter was chosen over the Vickers because for a given test force the Knoop pyramid produces a diagonal that is about three times as long and a depth of indentation that is about two-thirds of the values produced by the Vickers pyramid. Several different loads were used ranging from 5 to 200 grams. The length of the long diagonal was measured using the optical microscope. On every sample at least ten measurements were taken at each of the two lighter loads, eight measurements at each of the two middle loads, and six measurements at each of the two heavier loads to obtain statistically significant values. The two larger loads were used to monitor the hardness of the bulk chromium. This was done to insure that no effects of the implantation were observed on the hardness of the chromium plating. The lighter loads were used to evaluate the implanted layer and to estimate the depth of the modified layer. The measurements were taken on the top surface of the samples with the indenter perpendicular to the specimen, i.e., the indentation depth was parallel to the direction of the ion penetration.

The improvement in microhardness was more apparent at the lower loads since the indentation depth approached the implanted layer thickness. However, even at the lowest load employed, 5 grams, the indentation depth was large enough to include effects from the chromium substrate. Therefore, the improvement in hardness in the near surface regions is underestimated and the hardness values are more a qualitative measure of the implantation effects.

The scatter in hardness data increased at the lower loads because of inherently larger uncertainties associated with the measurement of smaller indents. The lighter load measurements also contain a higher degree of variation due to the increased effects of surface roughness on the indentation.

2.6 Wear and Friction Testing

Wear testing was performed using a pin-on-disk geometry in accordance with ASTM test method G-99. The testing was performed at Implant Sciences Corporation, Wakefield, MA, using an ISC-200PC Tribometer System. 3.2 mm diameter alumina balls were used as the pins to wear against the chromium plated disks. A schematic of the pin-on-disk type testing system is shown in Figure 2.2. Each test was conducted for 60 minutes with the ball rotating on the sample at a constant load of 50 grams and sliding velocity of 10 cm/sec. All testing was carried out at room temperature without lubrication. The friction coefficient was recorded during the wear testing. The wear rate measurements were calculated from the disk volume loss according to ASTM G-99 using the following equation:

$$\text{disk volume loss, mm}^3 = \frac{\pi\ (\text{wear track radius, mm})(\text{track width, mm})^3}{6\ (\text{sphere radius, mm})} \quad (2.1)$$

The depth of the wear track was measured using a Tencor Instruments Alphastep 100 profilometer with four traces taken on each sample.

2.7 SEM Examination

Scanning electron microscopy (SEM) was used to examine the surface of the implanted chromium plated samples. This was done to determine if any modifications

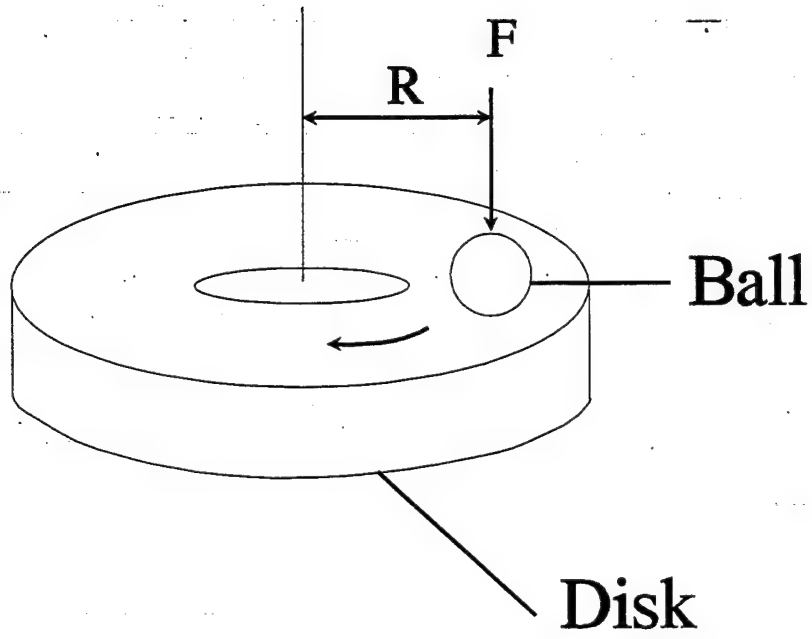

Figure 2.2 Schematic of pin-on-disk wear testing system. F is the normal force on the pin and R is the wear track radius.

to the surface were apparent due to the different doses or implantation processes used. SEM was also used to characterize the appearance of the wear tracks in both the unimplanted and implanted chromium plated samples.

3. RESULTS

3.1 Characterization of Hard Chromium and Low Contraction Chromium

Samples of both kinds of chromium were examined metallographically. In the as-polished condition, the hard chromium, shown in Figure 3.1, displayed microcracks throughout the plating that were not observed in the low contraction chromium plating, Figure 3.2. After etching the samples, the microstructure of the low contraction chromium displayed a fibrous grain structure, as shown in Figures 3.3a and b. The hard chromium microstructure, shown in Figures 3.4a and b, appeared to have a more directional, columnar grain structure than the low contraction chromium. The hard chromium plating was measured to have an average hardness of 850 KHN, Knoop hardness number, and the low contraction chromium had an average hardness of 450 KHN. Chemical analysis determined that the low contraction chromium was 99.92% chromium and the hard chromium was 99.97% chromium by weight percent. In both cases, chromium was the only element the instrumentation was able to measure.

3.2 Nitrogen and Argon Concentration Depth Profiles

The nitrogen and argon concentration depth profiles were measured by SIMS and AES. The graphs were analyzed and the results are shown in Tables 3.1 through 3.4. The range was measured from the surface of the sample to where the atomic concentration was at its maximum. The total depth measurement was made from the surface of the sample to the point where the ion concentration dropped below one atomic percent. The maximum concentration was measured to be the highest attained

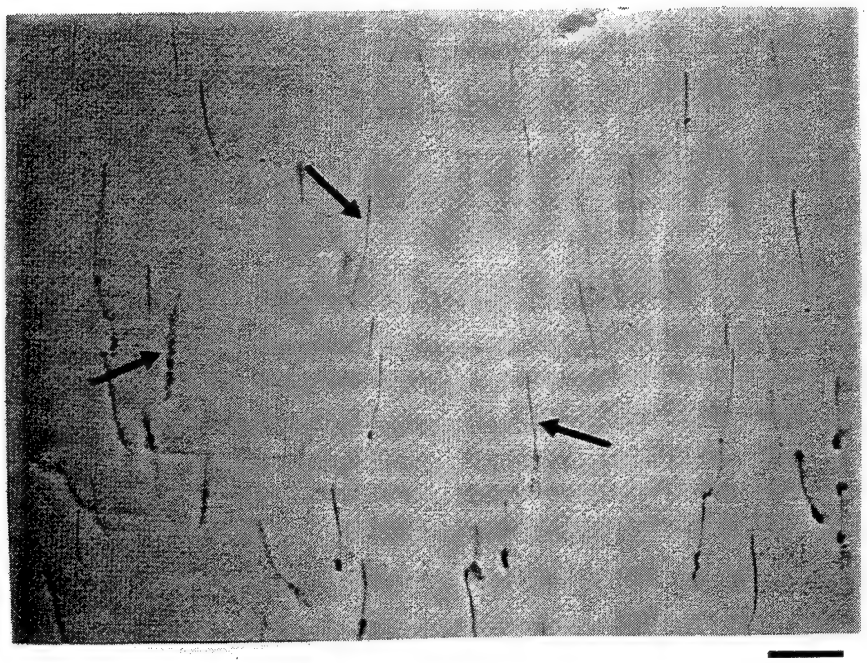

Figure 3.1 Cross-sectional micrograph of hard chromium plating. Sample shown in the as-polished condition. Arrows point to the microcracks present in the plating.

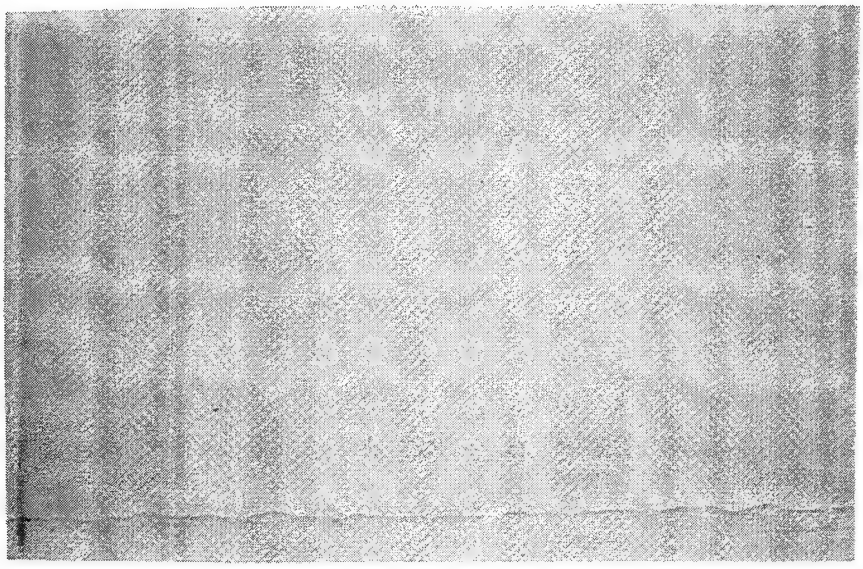

Figure 3.2 Cross-sectional micrograph of low contraction chromium plating. Sample shown in the as-polished condition.

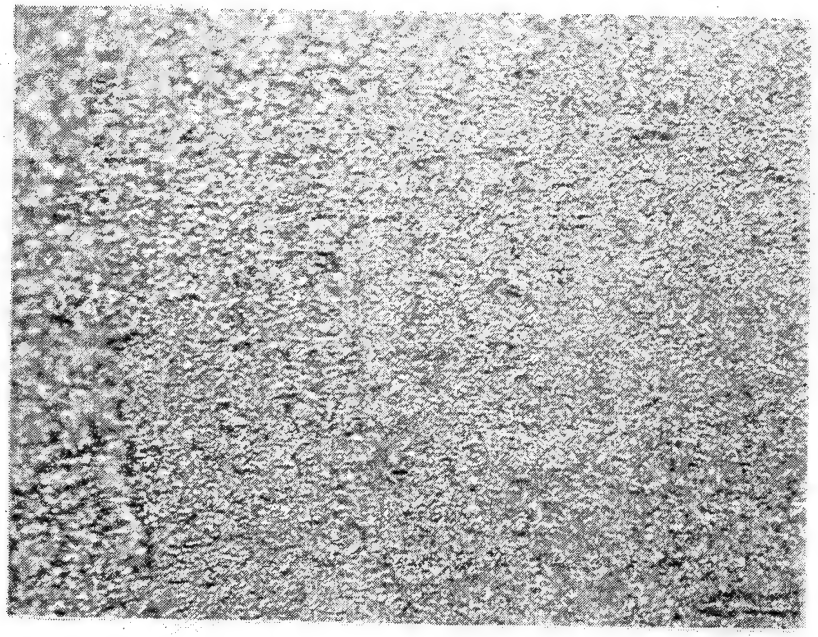

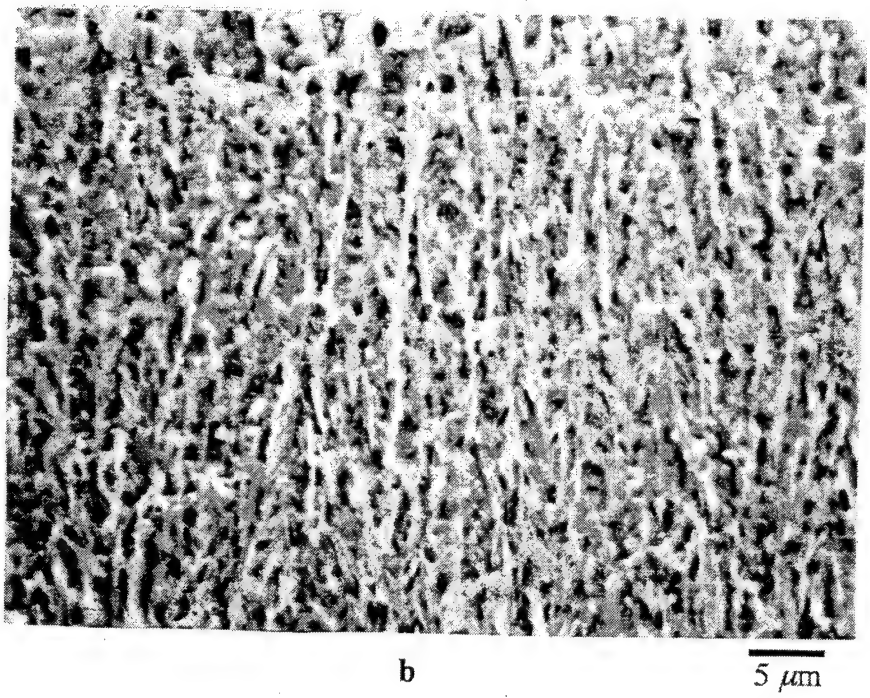

Figure 3.3 Microstructure of as-plated low contraction chromium depicting fibrous grain structure. a) is an optical photomicrograph and b) is an SEM micrograph. Etchant - 1 part HNO_3 and 3 parts HCl.

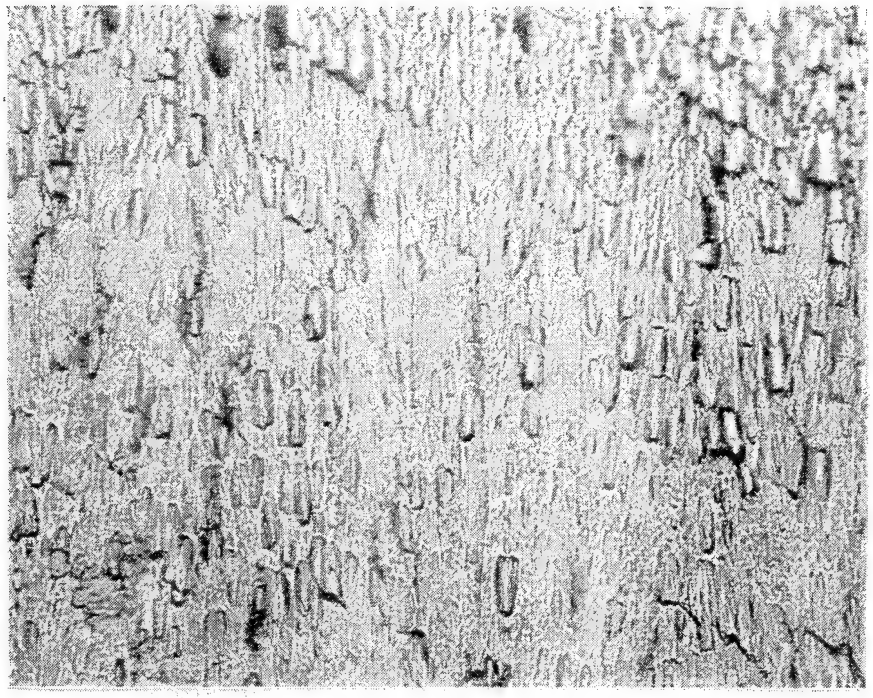

a 10 μm

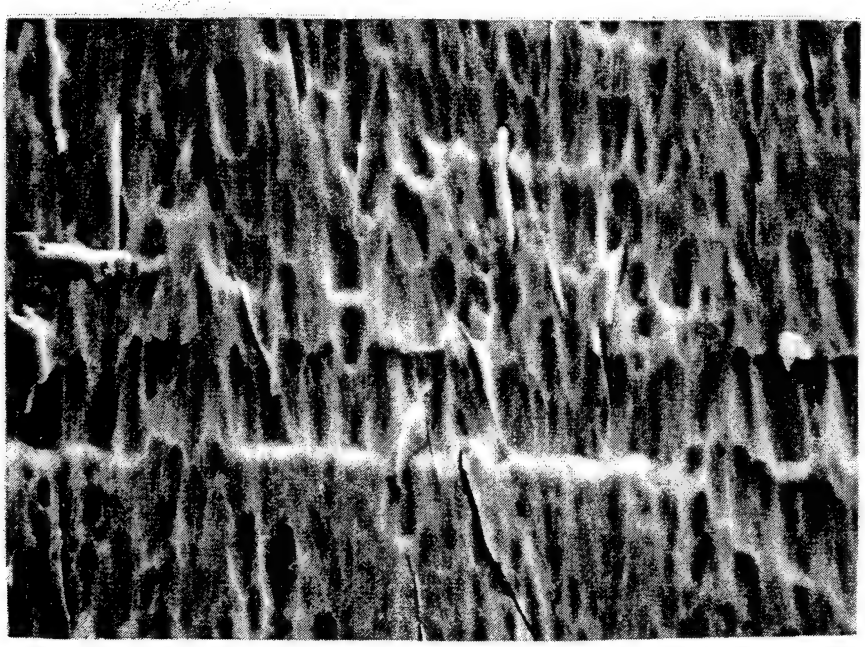

b 5 μm

Figure 3.4 Microstructure of as-plated hard chromium depicting coarse, columnar grain structure. a) is an optical photomicrograph and b) is an SEM micrograph. Etchant - 1 part HNO_3 and 3 parts HCl.

DOSE (ATOMS/CM^2)	IMPLANTATION TEMPERATURE	RANGE (Å)	TOTAL DEPTH (Å)	MAXIMUM CONCENTRATION (ATOMIC %)
9.4 x 10^{15}	Room Temp.	700	1200	2.8
9.4 x 10^{15}	500°C	600	1100	1.5
3.1 x 10^{16}	Room Temp.	700	1250	3.3
3.1 x 10^{16}	500°C	600	1200	4
3.1 x 10^{17}	Room Temp.	800	1800	39
3.1 x 10^{17}	500°C	950	2100	35
3.1 x 10^{18}	Room Temp.	1300	2200	43
3.1 x 10^{18}	500°C	1550	2800	39

Table 3.1 SIMS and AES Data for Nitrogen Implanted Hard Chromium

DOSE (ATOMS/CM^2)	IMPLANTATION TEMPERATURE	RANGE (Å)	TOTAL DEPTH (Å)	MAXIMUM CONCENTRATION (ATOMIC %)
9.4 x 10^{15}	Room Temp.	600	900	2.0
9.4 x 10^{15}	500°C	----	----	----
3.1 x 10^{16}	Room Temp.	650	1000	2.5
3.1 x 10^{16}	500°C	650	1100	4.0
3.1 x 10^{17}	Room Temp.	650	1450	22.0
3.1 x 10^{17}	500°C	650	1400	19.0
3.1 x 10^{18}	Room Temp.	1200	2100	41.0
3.1 x 10^{18}	500°C	1400	2500	40.0

Table 3.2 SIMS and AES Data for Nitrogen Implanted Low Contraction Chromium

DOSE (ATOMS/CM^2)	IMPLANTATION TEMPERATURE	RANGE (Å)	TOTAL DEPTH (Å)	MAXIMUM CONCENTRATION (ATOMIC %)
9.4 x 10^{15}	Room Temp.	250	600	2.5
9.4 x 10^{15}	500°C	250	600	3.0
3.1 x 10^{16}	Room Temp.	350	750	8.0
3.1 x 10^{16}	500°C	300	750	9.0
3.1 x 10^{17}	Room Temp.	----	----	----
3.1 x 10^{17}	500°C	300	750	6.0

Table 3.3 SIMS Data for Argon Implanted Hard Chromium

DOSE (ATOMS/CM^2)	IMPLANTATION TEMPERATURE	RANGE (Å)	TOTAL DEPTH (Å)	MAXIMUM CONCENTRATION (ATOMIC %)
9.4 x 10^{15}	Room Temp.	200	550	2.5
9.4 x 10^{15}	500°C	200	550	2.5
3.1 x 10^{16}	Room Temp.	250	800	8.0
3.1 x 10^{16}	500°C	300	800	8.0
3.1 x 10^{17}	Room Temp.	----	----	----
3.1 x 10^{17}	500°C	300	850	19.0

Table 3.4 SIMS Data for Argon Implanted Low Contraction Chromium

atomic percent value for the implanted ion.

In some of the samples, a distinct carbon film was observed on the surface of the implanted chromium. Figure 3.5 shows a typical example of this kind of film. For these samples, the position of the chromium surface was determined to begin where the chromium atomic percent concentration was 50%. The range and total

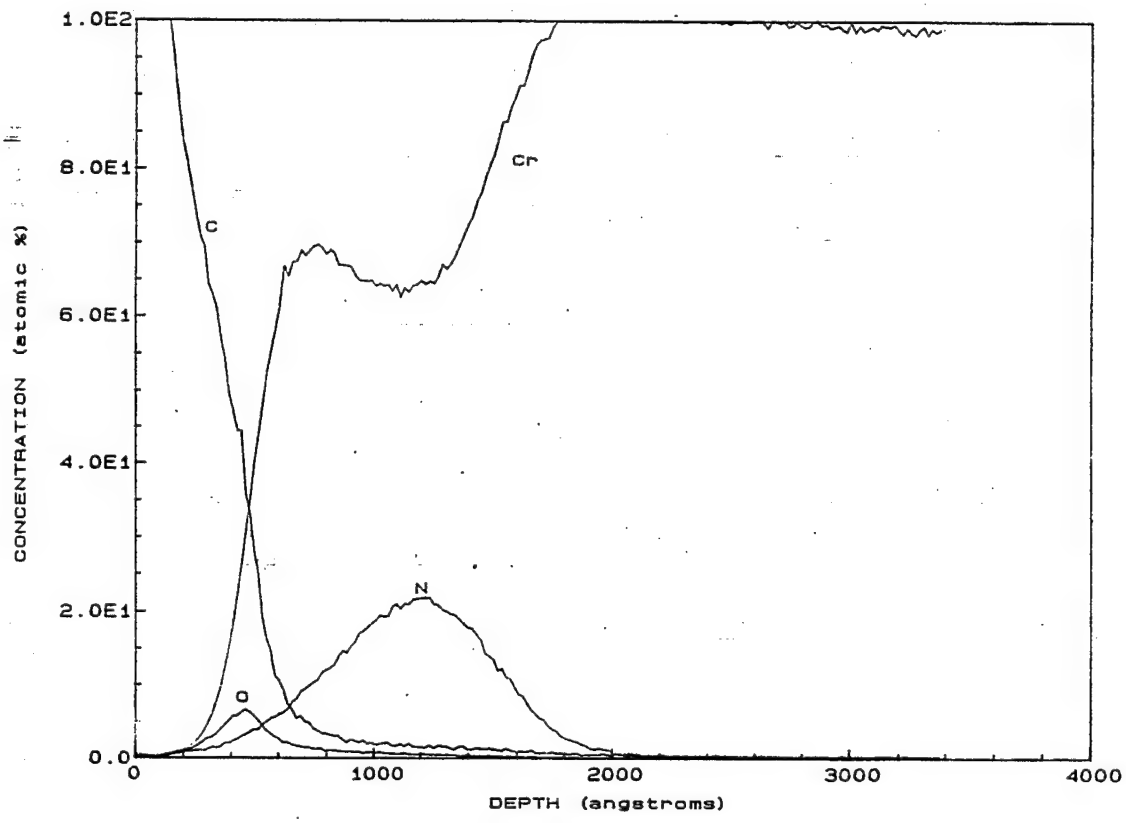

Figure 3.5 Nitrogen concentration depth profile showing carbon film on surface of sample. Sample was low contraction chromium plated and implanted with a dose of 3.1 x 10^{17} atoms/cm^2 at room temperature.

depth values were then measured from this position. The only exception to this rule was made for the samples implanted at the highest dose, 3.1×10^{18} atoms/cm^2. In these four samples, the carbon and oxygen seemed to be incorporated into the chromium surface and a distinct surface layer was not observed, as shown representatively in Figure 3.6. Therefore, in these samples, the values for the range and total depth were measured directly from the graphs without any correction factor.

In the nitrogen implanted samples, the range, total depth, and maximum concentration increased with an increasing dose. There was very little difference in the values obtained for the two lower doses measured. But, in the two higher doses, a substantial increase was observed compared to the lower dose values. The maximum atomic concentration increased from about 2% to 40%, while the range and total depth approximately doubled. A valid SIMS measurement for the low contraction chromium plated sample implanted with a dose of 9.4×10^{15} atoms/cm^2 at elevated temperature was not obtained.

In the argon implanted samples, the range remained approximately the same regardless of the implantation dose and temperature. The maximum atomic concentration did increase slightly at the two higher doses measured. In the two room temperature samples with a dose of 3.1×10^{17} atoms/cm^2, valid measurements from the SIMS graphs could not be obtained due to an unusually large amount of carbon present throughout the implanted region.

In both kinds of chromium, the shape of the ion distribution curves obtained were similar for each of the conditions tested. For example, an elevated temperature,

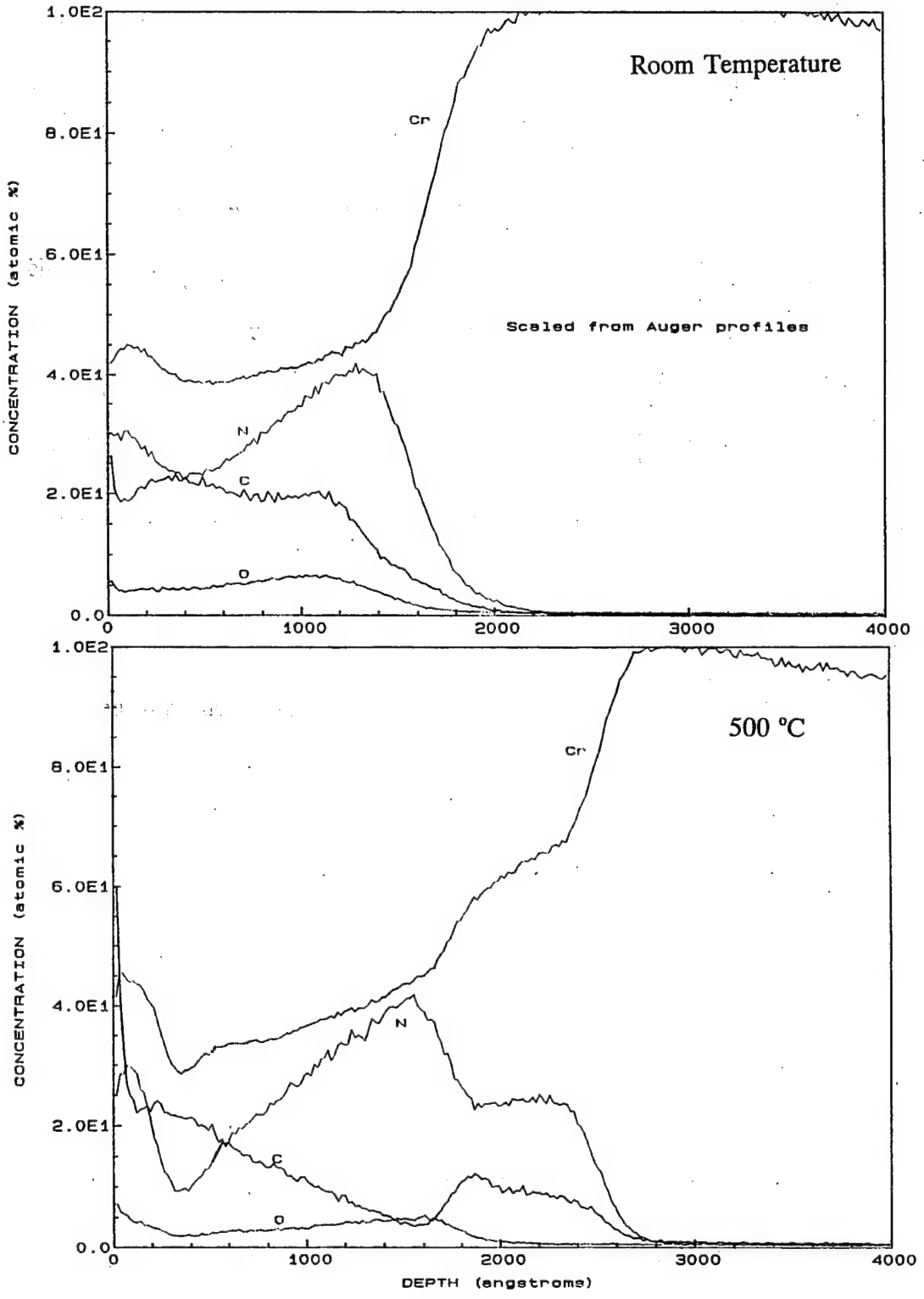

Figure 3.6 Nitrogen concentration depth profiles. The samples were low contraction chromium plated and implanted with a dose of 3.1 x 10^{18} atoms/cm^2 at a) room temperature and b) 500 °C.

hard chromium sample implanted at a dose of 3.1 x 10^{17} atoms/cm^2 had a similar shape nitrogen concentration depth profile as the low contraction chromium sample implanted at the same temperature and dose. The shapes of the nitrogen and argon concentration profiles, for the most part, were Gaussian (see Figure 3.5). The only notable exceptions were the samples implanted with nitrogen at the two highest doses measured.

For the 3.1 x 10^{17} atoms/cm^2 dose, the ion distribution curve broadened at the elevated temperature, Figure 3.7, as compared to the room temperature condition, shown previously in Figure 3.5. The sample showed nitrogen diffusion had occurred both toward the surface and into the sample. For both kinds of chromium, the maximum atomic concentration decreased slightly at the elevated temperature condition. This suggests that the elevated temperature implantation served to redistribute the nitrogen concentration within the samples.

At the highest implanted dose, 3.1 x 10^{18} atoms/cm^2, the distribution curves deviated considerably from Gaussian for both the room temperature and elevated temperature conditions. Figure 3.6 showed an example of the concentration profiles that were measured. In the room and elevated temperature samples, the nitrogen atomic percent concentration was much higher at the surface than in any of the lower dose samples. In the elevated temperature samples, there also seemed to be nitrogen diffusion occurring into the sample.

Retained dose measurements were also conducted on the highest dose nitrogen implanted samples. For the low contraction chromium, the retained dose was

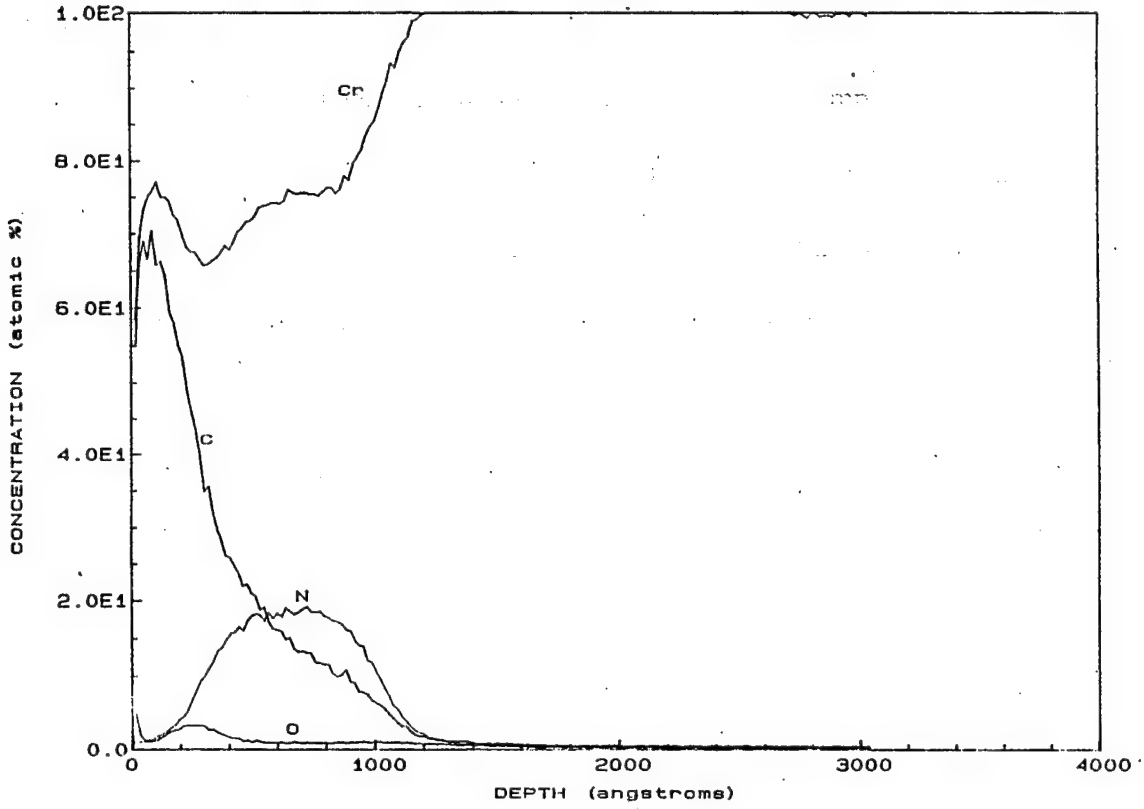

Figure 3.7 Nitrogen concentration depth profile. The sample was low contraction chromium plated and implanted with a dose of 3.1 x 10^{17} atoms/cm^2 at 500 °C.

measured to be 2.7 x 10^{17} atoms/cm^2 for the room temperature condition and 4.5 x 10^{17} atoms/cm^2 for the elevated temperature condition. For the hard chromium, the retained dose measurements were 4.6 x 10^{17} atoms/cm^2 and 5.3 x 10^{17} atoms/cm^2 for the room and elevated temperature conditions, respectively. In both kinds of chromium, the retained dose was slightly higher in the samples implanted at elevated temperature than the ones implanted at room temperature. For the same implantation conditions, the hard chromium samples appeared to have a slightly higher amount of retained nitrogen than the low contraction chromium samples.

Theoretical nitrogen and argon ion distribution curves were obtained by TRIM computer simulations and compared to the actual SIMS profiles. Figures 3.8 and 3.9 show the predicted range for ions with an energy of 75 keV implanted into pure chromium. The ion range for nitrogen was 926Å with a total depth of approximately 1800Å. Compared to the actual measurements, the simulation values most closely resemble the 3.1 x 10^{17} atom/cm^2 dose samples. The samples implanted with a lower dose are slightly below the predicted values and the samples implanted at a higher dose are slightly above. The ion range for argon was 385Å with a total depth of approximately 900Å. In all cases, the simulation predicted slightly higher values than were actually obtained in the samples.

3.3 Hardness Measurements

The Knoop microhardness was measured at various loads for both kinds of chromium and the results are displayed graphically in Figures 3.10 to 3.15. The error bars shown represent a 95% confidence level for the mean hardness values. In other

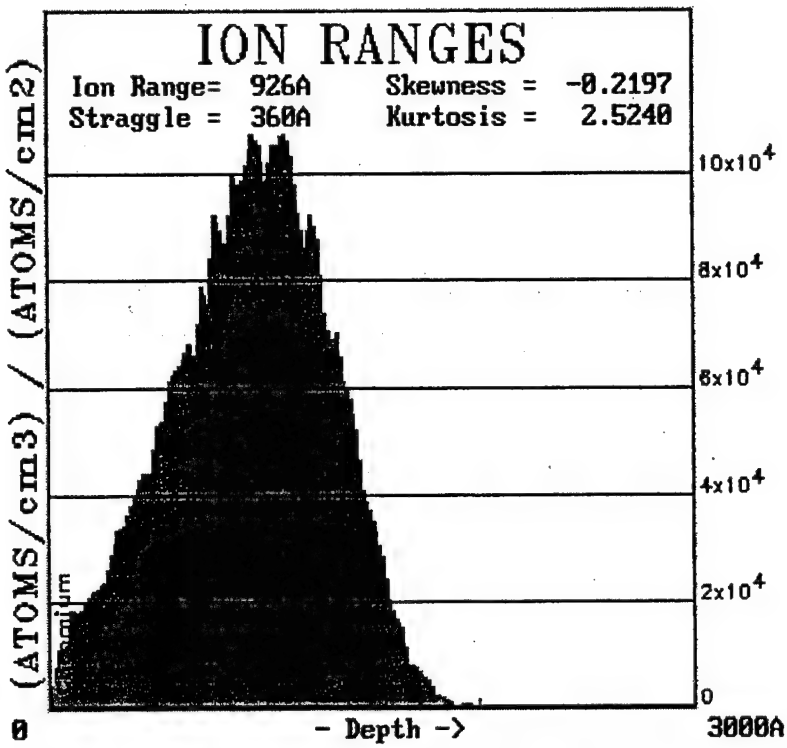

Figure 3.8 Ion range distribution of 75 keV nitrogen ions as obtained by TRIM computer simulation.

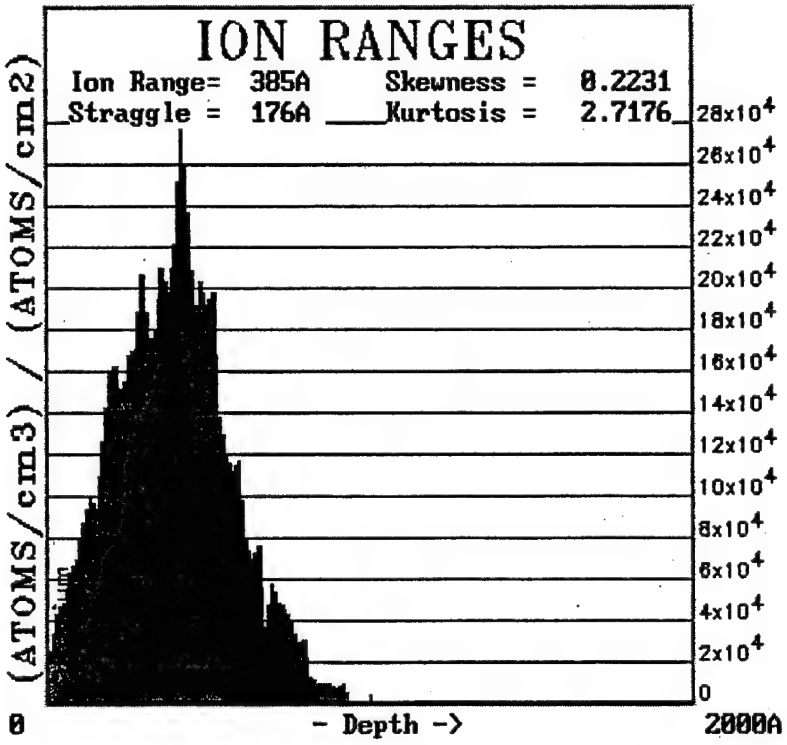

Figure 3.9 Ion range distribution of 75 keV argon ions as obtained by TRIM computer simulation.

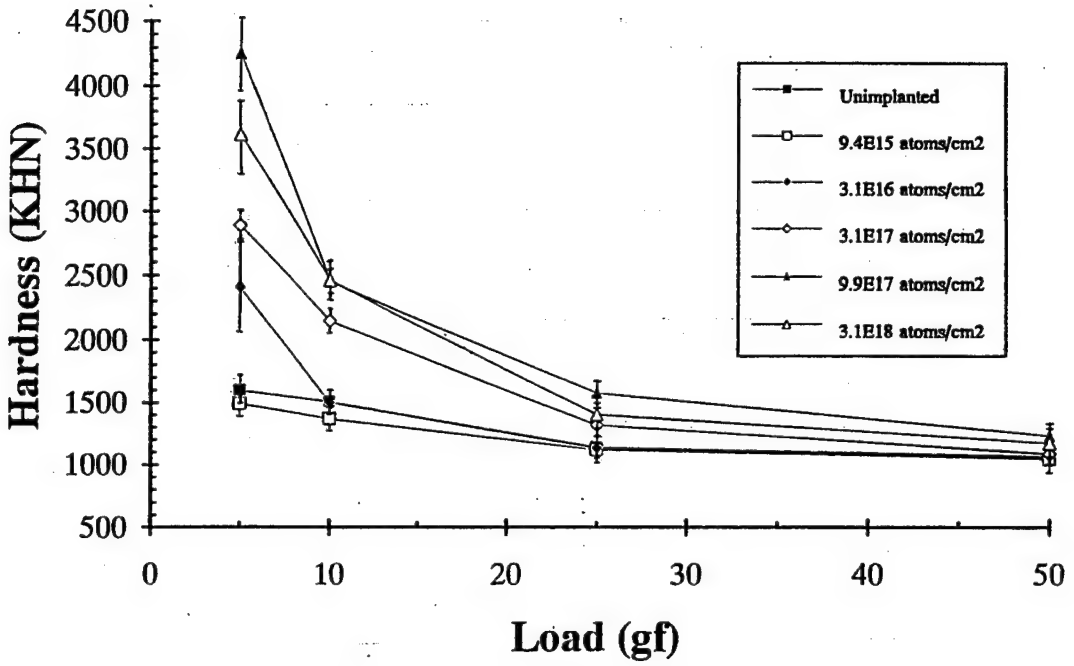

Figure 3.10 Knoop microhardness data for the room temperature, nitrogen implanted hard chromium. Error bars represent a 95% confidence level for the mean hardness.

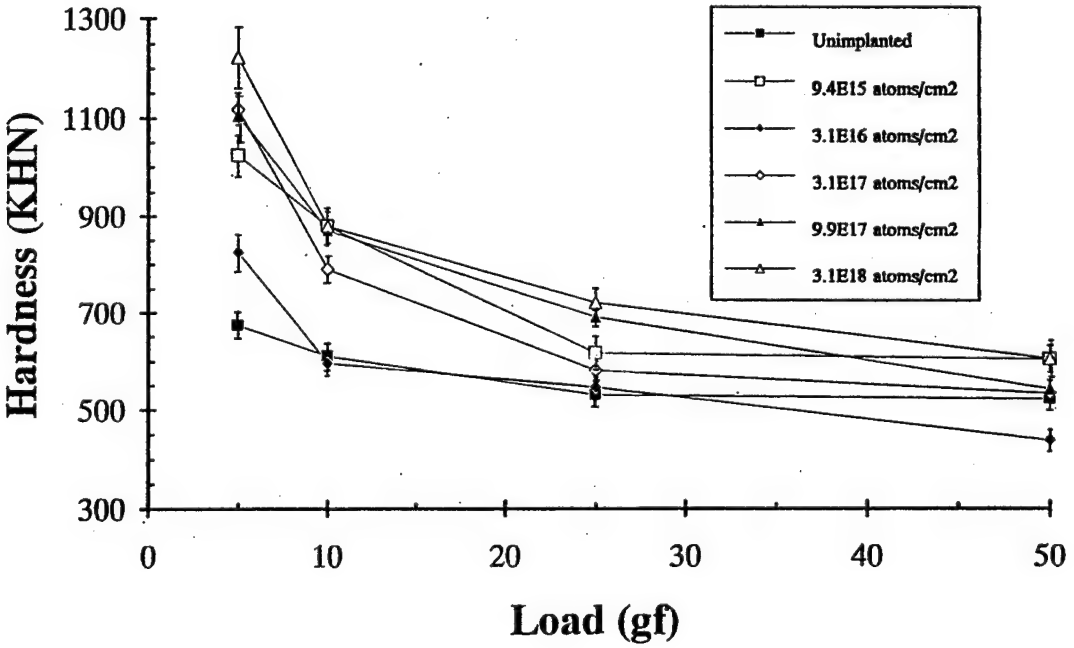

Figure 3.11 Knoop microhardness data for the room temperature, nitrogen implanted low contraction chromium. Error bars represent a 95% confidence level for the mean hardness.

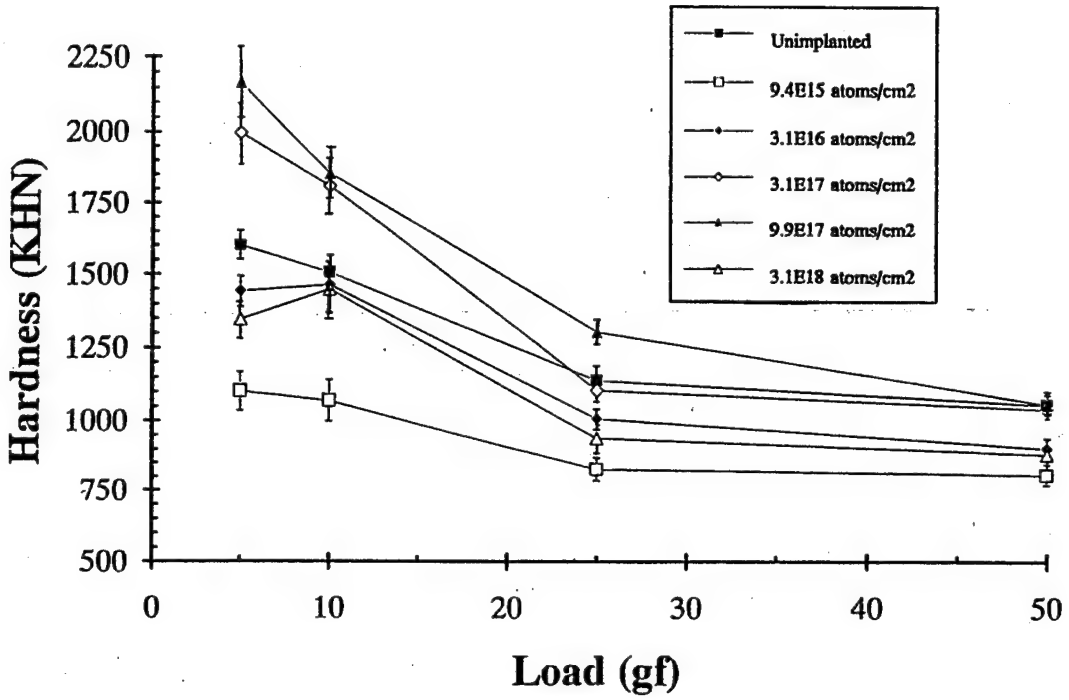

Figure 3.12 Knoop microhardness data for the elevated temperature, nitrogen implanted hard chromium. Error bars represent a 95% confidence level for the mean hardness.

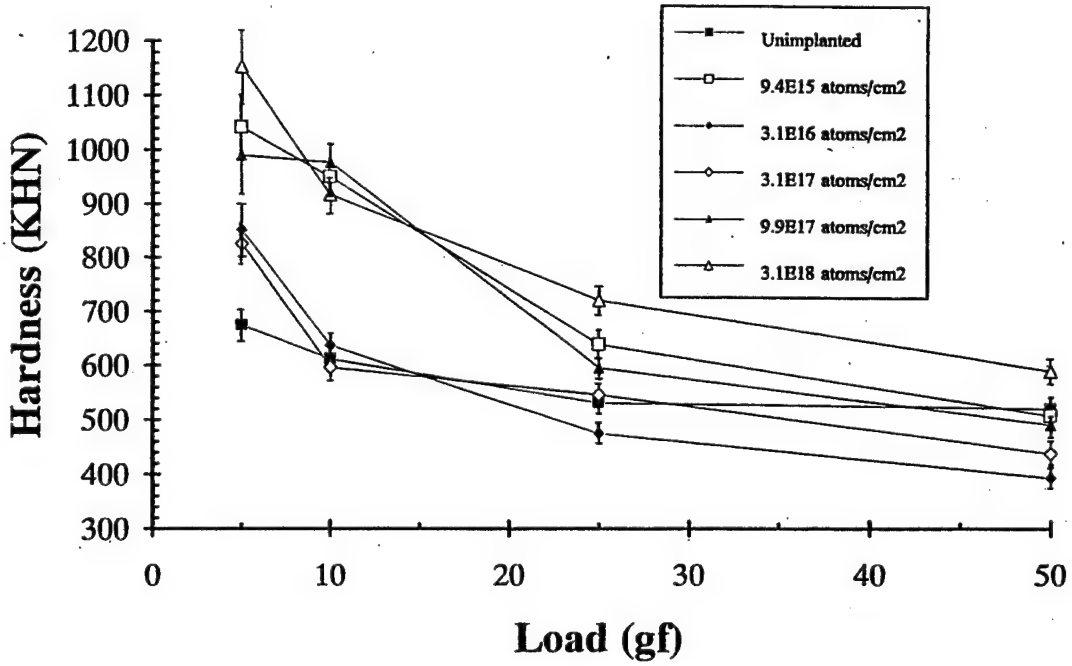

Figure 3.13 Knoop microhardness data for the elevated temperature, nitrogen implanted low contraction chromium. Error bars represent a 95% confidence level for the mean hardness.

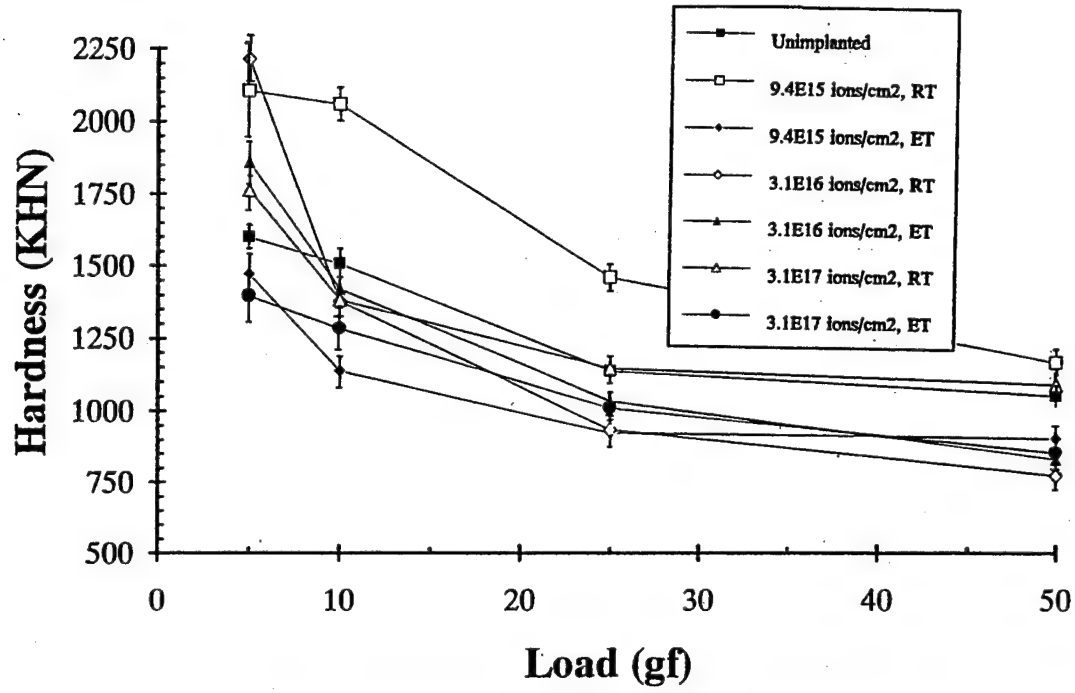

Figure 3.14 Knoop microhardness data for the argon implanted hard chromium. Error bars represent a 95% confidence level for the mean hardness.

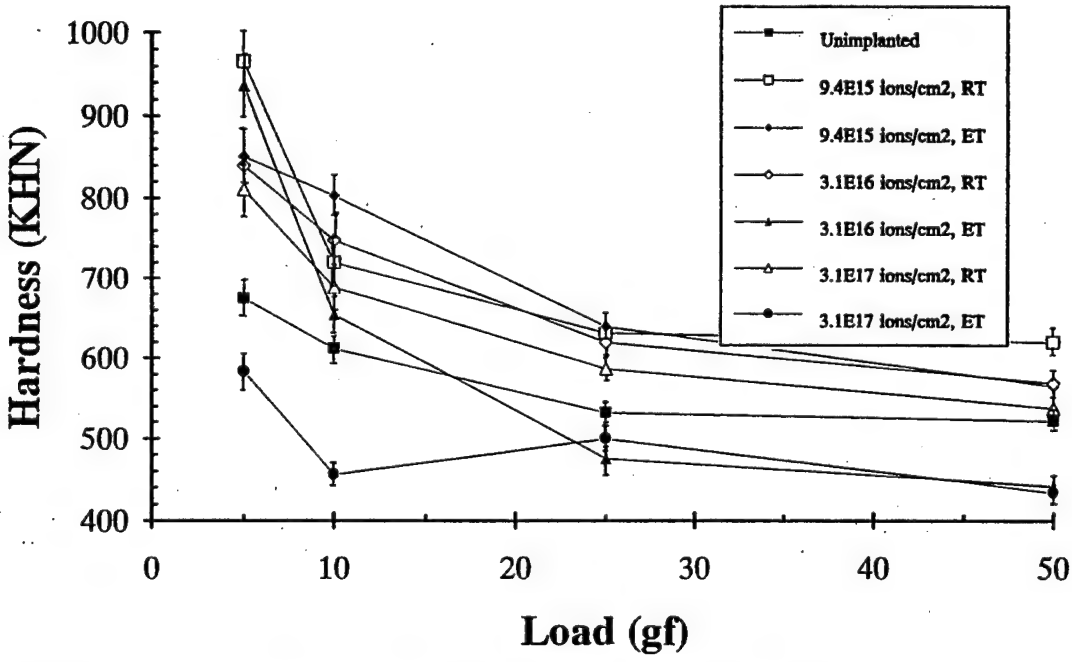

Figure 3.15 Knoop microhardness data for the argon implanted low contraction chromium. Error bars represent a 95% confidence level for the mean hardness.

words, with the hardness measurements obtained, 95 out of 100 times the mean will fall within the range shown. For the unimplanted chromium, the hardness increase observed at the lower loads is a known artifact of the hardness testing method[27].

The room temperature, nitrogen implanted samples displayed the largest increase in hardness in both kinds of chromium. For the hard chromium, in general, the hardness increased with an increasing dose. At the 5-gram load, the maximum hardness was obtained in the 9.9×10^{17} atoms/cm^2 dose sample. The hardness was increased to approximately three times the hardness of the unimplanted chromium. In the low contraction chromium, the trend of increasing hardness was somewhat less pronounced, although the three higher doses were the three hardest measured samples. At the 5-gram load, the maximum hardness was seen in the 3.1×10^{18} atoms/cm^2 dose which was slightly less than twice the hardness of the unimplanted sample.

In the elevated temperature, nitrogen implanted samples, there was a softening of the chromium observed in some cases. These samples were softer than the unimplanted chromium even at the heavier loads tested. This implies that the softening was likely due to the bulk chromium being affected by the elevated temperature condition rather than a result of the implantation process itself. Even with softening, some of these samples showed an increase in hardness at the lower loads. In the hard chromium, three of the five implanted samples displayed a softening of the chromium. For the two samples that seemed unaffected by the temperature, the hardness was increased with an increasing dose. At the 5-gram load, the maximum hardness was achieved at the 9.9×10^{17} atoms/cm^2 dose. The sample was

approximately 40% harder than the unimplanted chromium. In the low contraction chromium, two of the five implanted samples were affected by the elevated temperature. At the 5-gram load, the greatest increase in hardness was at the 3.1 x 10^{18} atoms/cm^2 dose. The sample was approximately 75% harder than the unimplanted chromium.

In the argon implanted chromium, most of the samples implanted at the elevated temperature observed a softening in the plating. In general, the hardness seemed to increase with a decreasing dose. In both kinds of chromium, the hardness was increased approximately 40% compared to the unimplanted chromium at the 5-gram load.

In most of the implanted samples, there was a substantial increase in hardness observed from the 200-gram load to the 5-gram load. The depth of the indentation at the 200-gram load was ~ 1.9 μm for the hard chromium and ~ 2.6 μm for the low contraction chromium. At the 5-gram load, the depth varied from ~ 0.14 to 0.22 μm for the hard chromium and ~ 0.26 to 0.34 μm for the low contraction chromium. Therefore, the 200-gram load primarily measured the hardness of the bulk chromium, while the 5-gram load measured the hardness of the chromium in the near surface. The increase in hardness at decreasing loads indicates that the surface region was much harder than the underlying region. Based on the SIMS and AES measurements, the thickness of the nitrogen implanted layer was about 0.10 to 0.28 μm. Therefore, even at the 5-gram load, the surface hardness is probably underestimated due to the contribution of the underlying, bulk chromium.

3.4 Friction and Wear Testing

The results of the disk volume loss and the friction coefficient measurements are shown in Tables 3.5 through 3.8. During the wear testing, most of the samples experienced a run-in period before settling to a relatively constant friction coefficient value. Figure 3.16 shows a typical plot of the measured coefficient of friction. There were, however, some samples that showed a continuously varying coefficient of friction. For these samples, the range of values observed was documented. A valid wear test was never obtained for the hard chromium sample implanted with nitrogen at a dose of 3.1×10^{16} atoms/cm^2 at elevated temperature.

The nitrogen implanted samples all experienced a decrease in the wear rate and coefficient of friction with increasing dose. The friction coefficient for both the hard chromium and the low contraction chromium was measured to be around $\mu \approx 0.50$ to 0.75 with an average of approximately 0.65. At the lower two doses tested, the elevated temperature samples seemed to have improved wear and friction characteristics compared to the room temperature samples at the same condition. Figure 3.17 shows the difference observed for a low contraction chromium sample implanted with a dose of 3.1×10^{17} atoms/cm^2 at elevated temperature as compared to the room temperature condition, shown previously in Figure 3.16. The greatest reduction in the friction coefficient was for the highest dose tested, 9.9×10^{17} atoms/cm^2, at both the room temperature and elevated temperature conditions. The coefficient of friction was reduced approximately 50% in both kinds of chromium.

The argon implanted samples all experienced the same or worse wear rate as

DOSE (ATOMS/CM^2)	IMPLANTATION TEMPERATURE	DISK WEAR (mm^3)	FRICTION COEFFICIENT, μ
Unimplanted	-----	0.0132	.50 - .75
3.1 x 10^{16}	Room Temp.	-----	-----
3.1 x 10^{16}	500°C	negligible	.45 - .55
3.1 x 10^{17}	Room Temp.	0.0154	.55
3.1 x 10^{17}	500°C	negligible	.37
9.9 x 10^{17}	Room Temp.	negligible	.28
9.9 x 10^{17}	500°C	negligible	.32 - .35

Table 3.5 Wear and Friction Data for Nitrogen Implanted Hard Chromium

DOSE (ATOMS/CM^2)	IMPLANTATION TEMPERATURE	DISK WEAR (mm^3)	FRICTION COEFFICIENT, μ
Unimplanted	-----	0.0194	.55 - .70
3.1 x 10^{16}	Room Temp.	0.0146	.62
3.1 x 10^{16}	500°C	0.0283	.57
3.1 x 10^{17}	Room Temp.	0.0269	.62
3.1 x 10^{17}	500°C	negligible	.4
9.9 x 10^{17}	Room Temp.	negligible	.31
9.9 x 10^{17}	500°C	negligible	.26 - .34

Table 3.6 Wear and Friction Data for Nitrogen Implanted Low Contraction Chromium

DOSE (ATOMS/CM^2)	IMPLANTATION TEMPERATURE	DISK WEAR (mm^3)	FRICTION COEFFICIENT, μ
Unimplanted	-----	0.0132	.50 - .75
3.1 x 10^{16}	Room Temp.	0.0221	.50 - .65
3.1 x 10^{16}	500°C	0.0675	.30* → .55 - .70
3.1 x 10^{17}	Room Temp.	0.0256	.50 - .70
3.1 x 10^{17}	500°C	0.0296	.20 - .40* → .60 - .70

Table 3.7 Wear and Friction Data for Argon Implanted Hard Chromium.
* Denotes sample experienced a breakthrough of the implanted layer.

DOSE (ATOMS/CM^2)	IMPLANTATION TEMPERATURE	DISK WEAR (mm^3)	FRICTION COEFFICIENT, μ
Unimplanted	-----	0.0194	.55 - .70
3.1 x 10^{16}	Room Temp.	0.0233	.33* → .55 - .70
3.1 x 10^{16}	500°C	0.0188	.57 - .70
3.1 x 10^{17}	Room Temp.	0.0208	.55 - .60
3.1 x 10^{17}	500°C	0.0160	.62 - .70

Table 3.8 Wear and Friction Data for Argon Implanted Low Contraction Chromium.
* Denotes sample experienced a breakthrough of the implanted layer.

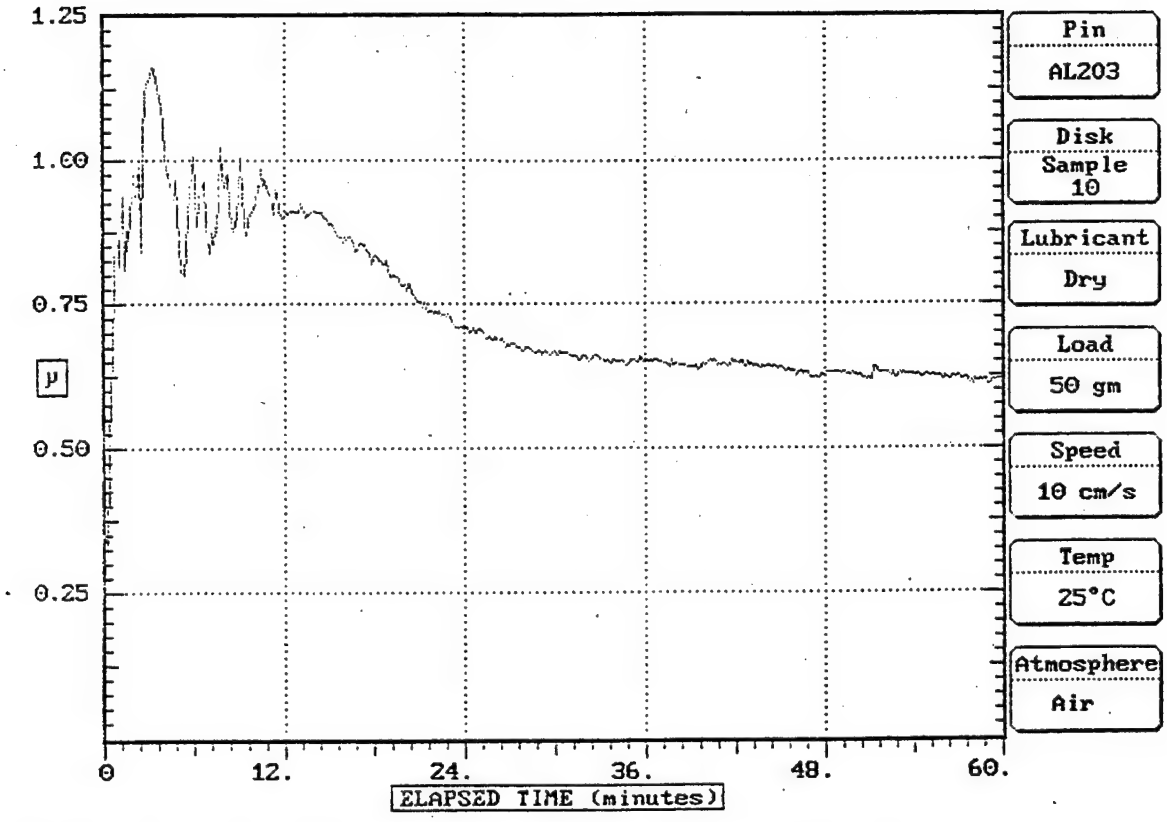

Figure 3.16 Typical friction coefficient plot. The sample was low contraction chromium plated and implanted with nitrogen at room temperature with a dose of 3.1×10^{17} atoms/cm^2.

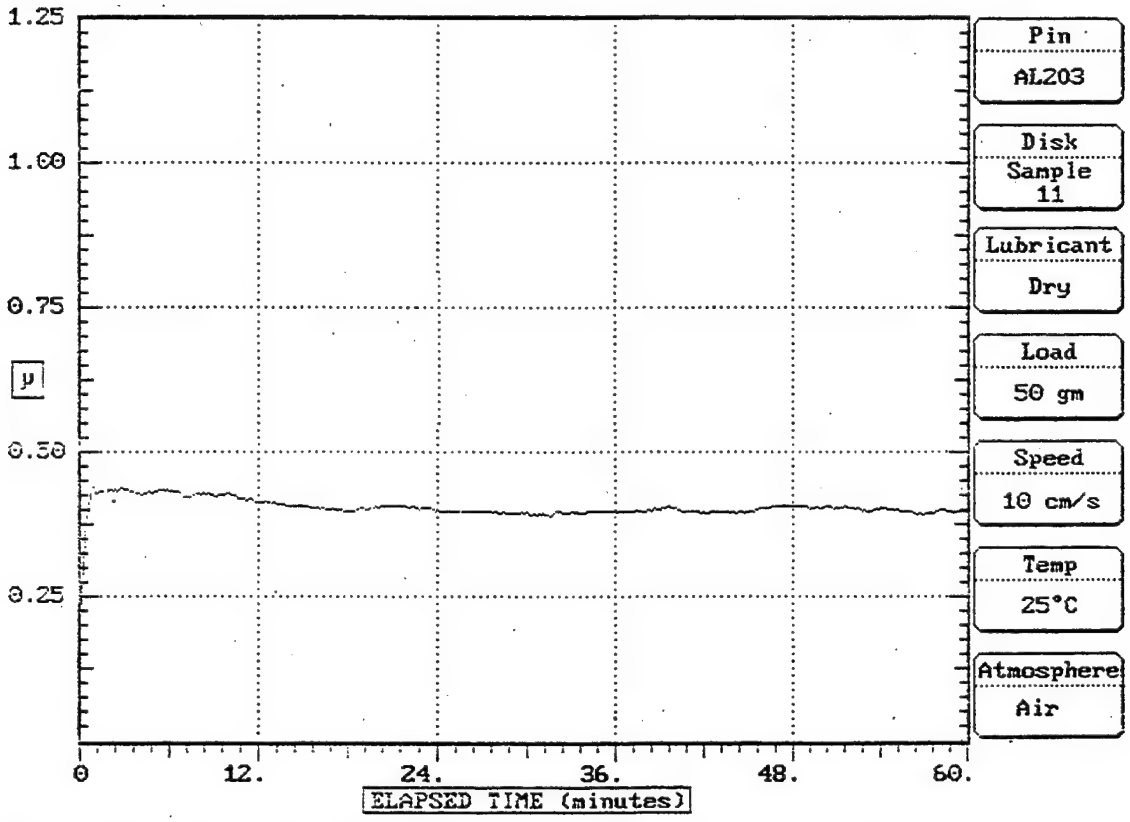

Figure 3.17 Friction coefficient plot for a low contraction chromium sample implanted with nitrogen at 500 °C with a dose of 3.1 x 10^{17} atoms/cm^2.

the unimplanted samples. Three of the samples did display an initial improvement in the friction coefficient before a breakthrough of the implanted layer occurred. Breakthrough is characterized by a sharp increase in the friction coefficient with the value returning to that of the unimplanted chromium. Figure 3.18 shows a breakthrough of the implanted layer at approximately 7 to 8 minutes into the wear test. The two elevated temperature, hard chromium samples, with a dose of 3.1×10^{16} and 3.1×10^{17} atoms/cm^2, experienced breakthrough at 2 to 3 minutes and 40 minutes into the wear test, respectively. The remaining samples showed no improvement in the friction coefficient.

Optical profilometry was conducted on selected samples to further characterize the wear tracks. Figures 3.19 and 3.20 show the difference in wear observed for two nitrogen implanted, hard chromium samples. Figure 3.19 shows the wear track for a sample implanted at room temperature with a dose of 3.1×10^{17} atoms/cm^2. Figure 3.20 shows the negligible wear observed for a sample implanted at room temperature with a dose of 9.9×10^{17} atoms/cm^2.

3.5 SEM Examination

The surface of the implanted chromium plated samples was examined using a scanning electron microscope. The only notable feature that was observed was the presence of bubbles in the two higher-dose, 9.9×10^{17} atoms/cm^2 and 3.1×10^{18} atoms/cm^2, nitrogen implanted samples. Figure 3.21 shows a representative SEM micrograph depicting this feature. Bubbles were seen on the room temperature samples, but were not observed on the elevated temperature samples.

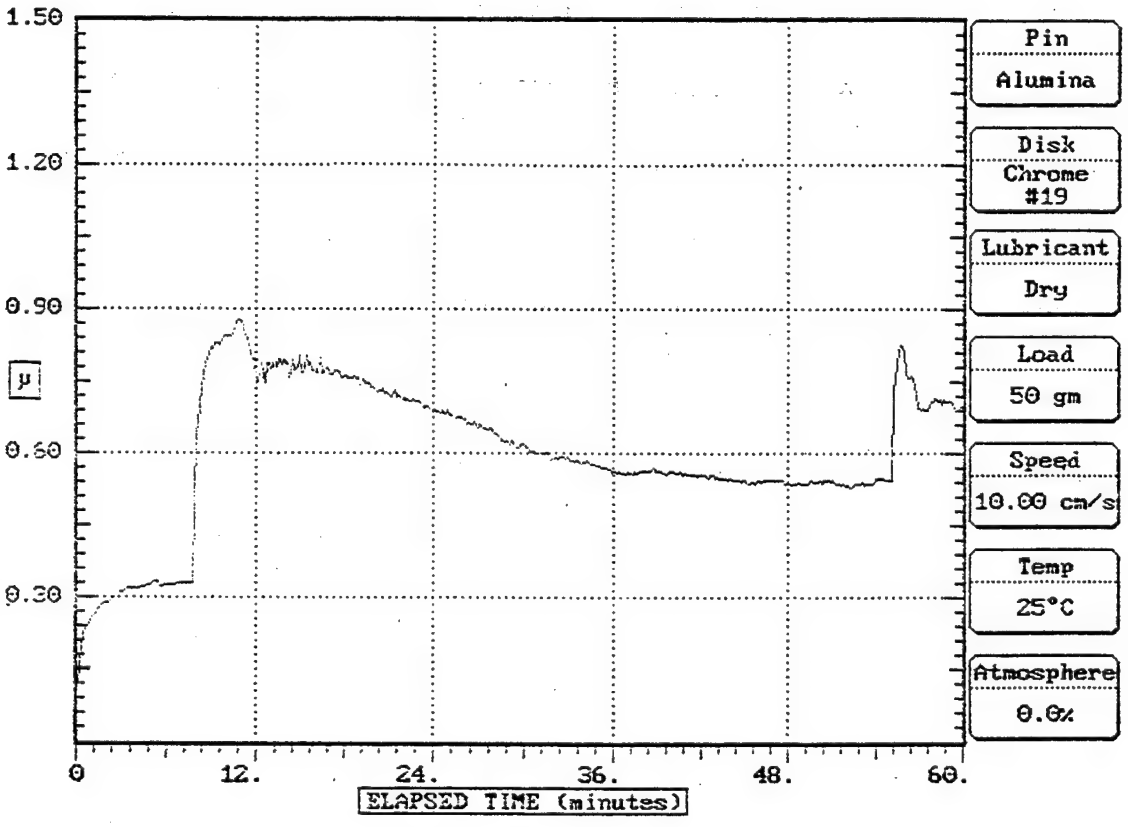

Figure 3.18 Friction coefficient for an argon implanted sample displaying break-through of the implanted layer at approximately 7 - 8 minutes into the wear test. The sample was plated with low contraction chromium and implanted at room temperature with a dose of 3.1×10^{16} atoms/cm^2.

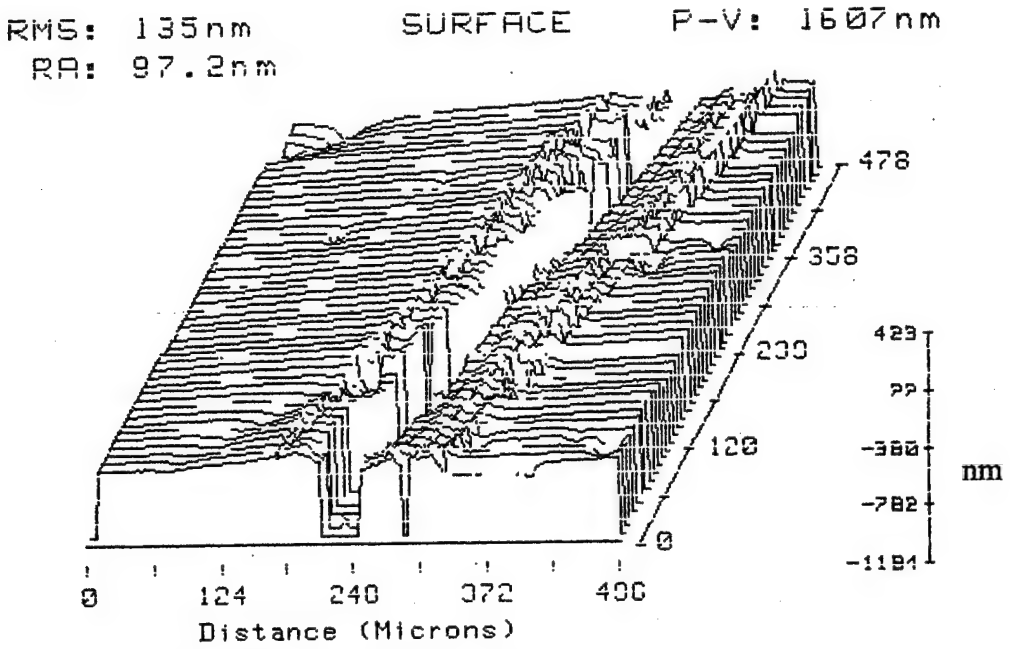

Figure 3.19 Optical profilometry of a sample that had experienced measurable disk volume loss during wear testing. The sample was hard chromium plated and implanted with nitrogen at room temperature and a dose of 3.1 x 10^{17} atoms/cm^2.

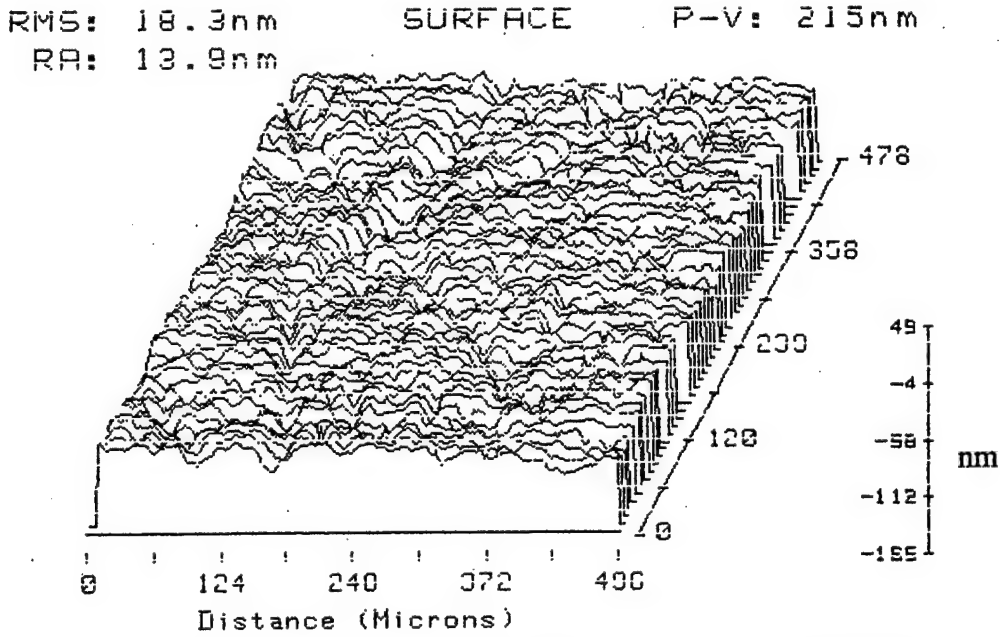

Figure 3.20 Optical profilometry of a sample that had experienced negligible disk volume loss during wear testing. The sample was hard chromium plated and implanted with nitrogen at room temperature and a dose of 9.9 x 10^{17} atoms/cm^2.

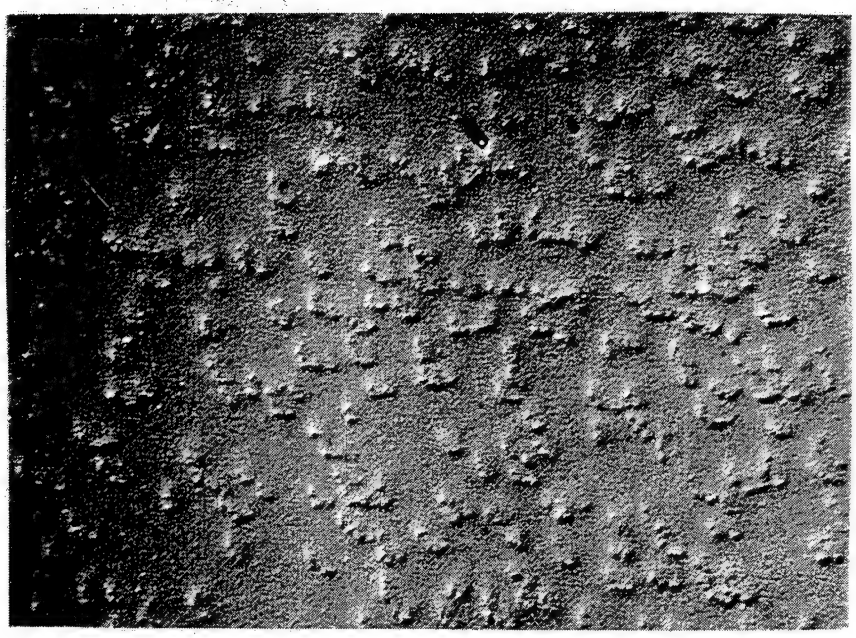

Figure 3.21 SEM micrograph of the bubbles observed on the surface of the higher dose, room temperature, nitrogen implanted samples.

The appearance of the wear track was also examined using an SEM. In the samples that displayed measurable wear, the low contraction chromium and hard chromium wear tracks displayed similar appearances to their unimplanted samples. Figures 3.22 and 3.23 show typical SEM micrographs of the worn surfaces for both low contraction and hard chromium, respectively. In the samples that displayed negligible wear, the surface appeared to be slightly affected by the wear testing. Samples plated with both kinds of chromium displayed only small grooves in the wear track. Figures 3.24 and 3.25 show the relatively negligible wear observed on the surface of a low contraction chromium and hard chromium plated surface, respectively.

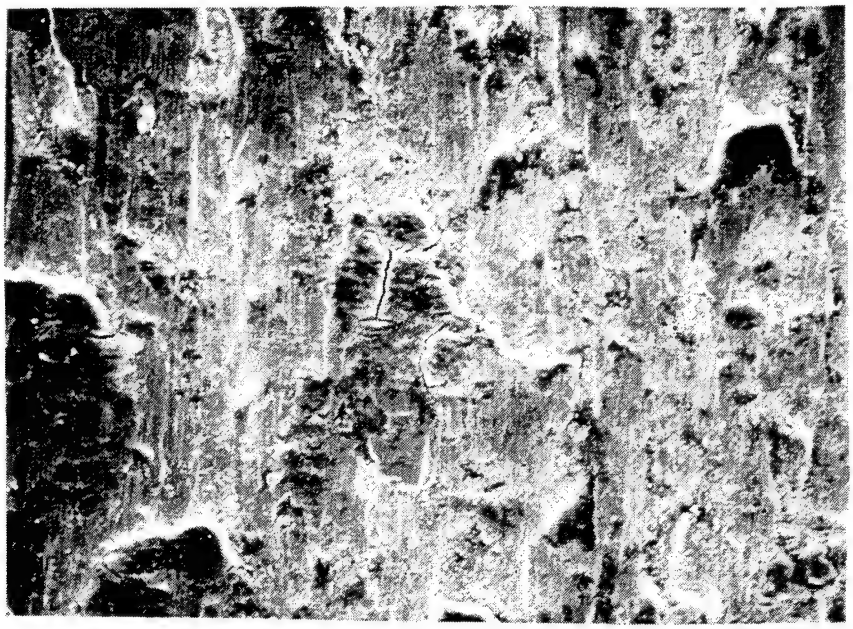

Figure 3.22 Typical SEM micrograph of the worn low contraction chromium surface after wear testing for 60 minutes with a 50 gram load at 10 cm/sec.

Figure 3.23 Typical SEM micrograph of the worn hard chromium surface after wear testing for 60 minutes with a 50 gram load at 10 cm/sec.

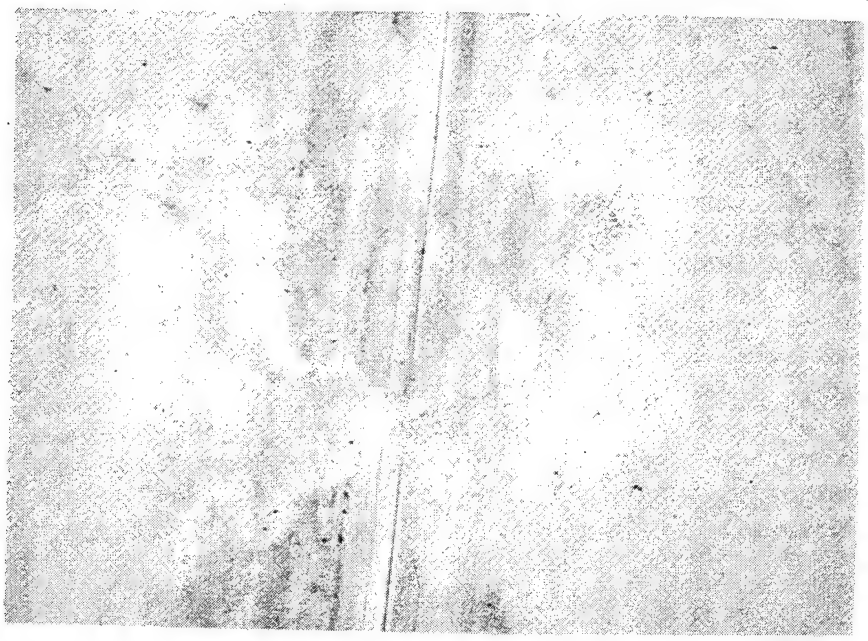

Figure 3.24 SEM micrograph of the wear track in the nitrogen implanted low contraction chromium plating. The sample was implanted with a dose of 3.1 x 10^{17} atoms/cm^2 at an implantation temperature of 500 °C.

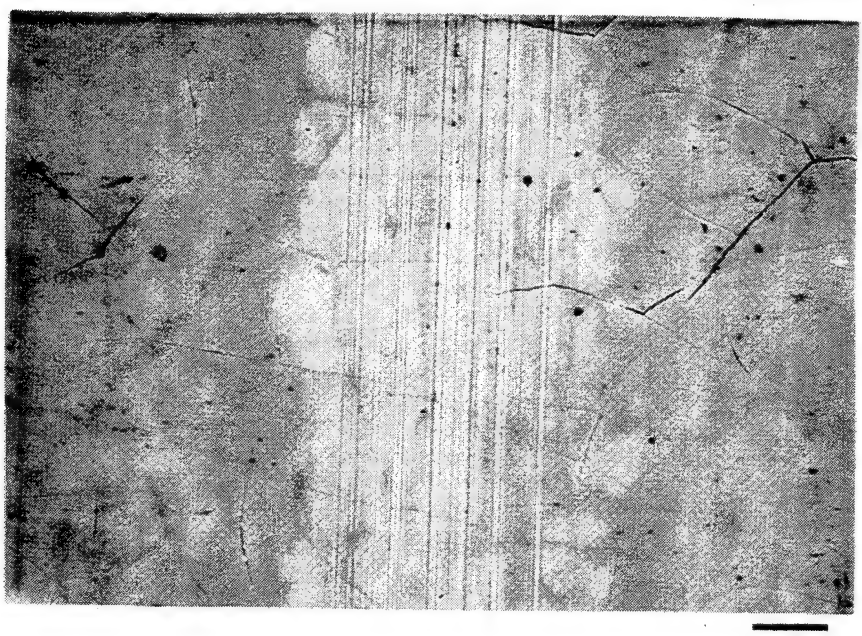

Figure 3.25 SEM micrograph of the wear track in the nitrogen implanted hard chromium plating. The sample was implanted with a dose of 3.1 x 10^{16} atoms/cm^2 at an implantation temperature of 500 °C.

4. DISCUSSION OF RESULTS

An improvement in the surface properties of ion implanted electroplated chromium was observed for a number of different process conditions. Based on the results obtained in this research, several observations can be made.

4.1 Effects of Ion Species

The hardness, friction, and wear properties were all improved with the implantation of nitrogen at sufficiently high ion doses. For the samples implanted with argon, there was no improvement in the wear resistance, an initial improvement in the friction coefficient for three samples, and a slight increase in the surface hardness. Therefore, the improvement in properties can most likely be attributed to a chemical effect occurring between the chromium and nitrogen rather than an effect produced by the implantation process itself. This observation has been supported by several researchers[18,28,29] who have found the presence of chromium nitrides, CrN or Cr_2N, in nitrogen implanted electroplated chromium. Unfortunately, there is not universal agreement as to the mechanisms behind these improved properties. A number of theories have been suggested in the literature and are discussed below.

Onate et al.[18] suggested that the increase in hardness was the result of precipitation hardening rather than interstitial or solid solution hardening. They stated that chromium nitrides were 50% harder than the bulk hard chromium. Hutchings[30], however, proposed that the increase in hardness was the result of solid solution

hardening, the formation of nitride layers, and precipitation hardening. Oliver et al.[31] similarly suggested that the hardness increase may be attributed to residual stress, interstitial hardening, as well as nitride precipitation. According to the results found in this report, there are definitely contributions from mechanisms other than just precipitation hardening and nitride formation. The approximately 40% increase in hardness observed for the argon implanted samples supports this claim. Whether the increase is from interstitial or solid solution hardening, the stress induced in the surface due to the lattice strain, or another mechanism cannot be determined from the results obtained here. The majority of the improvement observed in the nitrogen implanted samples is, however, most likely due to the formation of nitride layers and precipitation hardening.

There are also differing theories as to the reasons behind the improvement in wear properties. Xie et al.[12] proposed that the wear resistance was improved due to the nitrides being effective at pinning dislocations, whereas Hutchings[30] proposed that the volume expansion associated with nitride formation produced residual stresses in the surface of the hard chromium thereby closing the surface microcracks. The results obtained in the present research do not support Hutchings' theory. Similar improvements in the wear and friction properties were observed for both the hard chromium and the relatively crack-free, low contraction chromium. Therefore, the closing of microcracks is most likely not the dominant wear improvement mechanism.

4.2 Effects of Ion Dose

In general, the hardness, friction, and wear properties were improved with an

increasing nitrogen dose. This trend has also been reported by several authors in the literature[18,32,33]. In the present research, the two highest doses, 9.9 x 10^{17} atoms/cm^2 and 3.1 x 10^{18} atoms/cm^2, displayed the greatest improvement in hardness for the hard chromium, and the highest dose showed the greatest improvement for the low contraction chromium. The maximum increase in hardness was observed at the 5-gram load for the room temperature, nitrogen implanted samples. A hardness improvement of three times that of the unimplanted hard chromium and slightly less than twice that of the unimplanted low contraction chromium was measured. This increase is slightly higher than the 1.4 to 2.6 improvement factor reported by some researchers[18,32,33]. A possible explanation for this may be the different hardness methods used or a lighter testing load employed. As mentioned previously, the Knoop microhardness indenter, for a given test force, produces a diagonal that is about three times as long and a depth of indentation that is about two-thirds of the values produced by the Vickers indenter. Therefore, at a similar gram force, the Vickers indenter is measuring more of the underlying, unimplanted chromium than the Knoop indenter. A higher testing load may also give less significant increases in hardness. In the research by Ferber et al.[32], they used a Knoop diamond indenter with a 10-gram load and saw about a 1.6 factor of improvement. Their increase in hardness is similar to that observed for the 10-gram load in the present research.

The greatest improvement in the friction coefficient was observed for the highest dose tested, 9.9 x 10^{17} atoms/cm^2. The coefficient of friction for both kinds of chromium was reduced by approximately 50%. In the wear testing, the two highest

doses, 3.1 x 10^{17} and 9.9 x 10^{17} atoms/cm^2, exhibited negligible wear. Comparison of these results with other research was extremely difficult. Friction coefficient values and wear loss measurements are sensitive to the load, speed, temperature, and lubrication condition used in the wear test. Similar results cannot be extrapolated from differing test conditions. Some of the improvements observed in the literature for hard chromium are mentioned below. Oliver et al.[31] observed a wear rate decrease of at least a factor of 20 with a 5-mm ball at a velocity of 5.65 x 10^{-2} m/s^2 at loads of 5.2 and 10.5 N. Onate et al.[18] saw a reduction factor in the wear resistance of about four times under lubricated test conditions at a 710 N load. Fischer et al.[20] observed a 31% wear reduction and a 7% coefficient of friction reduction using a 7.94-mm ball at a load of 8.3 N with a mean sliding velocity of 20 mm/s.

The maximum atomic concentration was increased with an increasing dose. In similar research conducted on nitrogen implanted electroplated chromium[18,32,33], the maximum concentration was found to be approximately 35 to 45 at%. These reported values are in close agreement with the results obtained in this report. The shape of the nitrogen concentration profile was also affected by the ion dose. At the highest dose, 3.1 x 10^{18} atoms/cm^2, the profile no longer appeared Gaussian, see Figure 3.6. The samples contained a higher concentration of nitrogen at the surface than any of the lower dose samples. Using an estimated sputtering yield of 0.3[34,35,36], at this dose approximately 500 to 650 Å of material would be removed. With the range being about two to three times this depth, the change in shape could not be accounted for by sputtering effects alone. A possible explanation for the shape is the effects of

radiation-enhanced diffusion. This would account for the preferential diffusion of nitrogen toward the surface that was not observed in any of the lower dose samples. This theory is also supported by the increased amount of oxygen and carbon mixing observed in the surface of these samples.

4.3 Effects of Implantation Temperature

A change in the ion concentration profile at elevated temperature implantation compared to room temperature has been well documented[12,13,14]. In this research, nitrogen diffusion was observed in the two highest doses tested, 3.1×10^{17} and 3.1×10^{18} atoms/cm^2, at the elevated temperature condition. In the lower dose, a broadening and flattening out of the nitrogen concentration profiles was observed compared to the room temperature samples. In the higher dose, the elevated temperature condition showed significant diffusion of nitrogen into the sample that was not observed in the room temperature conditions.

For the intermediate doses examined, 3.1×10^{16} and 3.1×10^{17} atoms/cm^2, the elevated temperature, nitrogen implanted samples appeared to have improved friction and wear properties, in some cases, as compared to the room temperature samples implanted at the same conditions. It has been suggested[12] that the improvement may be the result of the broadened distribution in these samples or the presence of more stable nitrides formed during the high temperature implantations. The properties may also have been affected by the softening observed in the base chromium as a result of the elevated temperature implantation.

4.4 Effects on Microstructure

For the most part, the observed effects of ion implantation on the hardness, friction, and wear properties were the same for both kinds of chromium. The only notable exception was the improvement in hardness for the nitrogen implanted, room temperature condition. In the hard chromium, the hardness increased approximately three times that of the unimplanted sample, whereas the low contraction chromium increased slightly less than twice that of the unimplanted sample. The only other difference observed in the two kinds of chromium was that the amount of retained nitrogen was slightly higher in the hard chromium as compared to the low contraction chromium.

5. CONCLUSIONS

The effects of ion implantation on two kinds of electroplated chromium have been studied. Both hard chromium and low contraction chromium were implanted with nitrogen or argon at both room temperature and 500°C. The hardness, wear, and friction properties were examined in the resulting films. The ion concentration depth profiles were also measured in order to characterize the implanted films. Scanning electron microscopy was used to examine the surface of the implanted chromium and to further characterize the wear tracks.

The greatest improvement in the properties was observed for the nitrogen implantations. This was attributed to the formation of chromium nitrides in the implanted films. In general, the hardness, wear, and friction properties improved with an increasing nitrogen dose. At the intermediate doses tested, some of the elevated temperature, nitrogen implanted samples showed improved friction and wear properties compared to the room temperature samples implanted at the same condition. The improvement may be attributed to a broadening of the nitrogen concentration profile observed in these samples. The elevated temperature implantations also appeared to decrease the hardness of the bulk chromium. For the room temperature samples, the maximum increase in hardness was observed at the 5-gram load for the nitrogen implanted samples. The hardness was increased three times that of the unimplanted hard chromium and slightly less than twice that of the unimplanted low contraction chromium. It was determined that the improvement in hardness was most likely due to the formation of nitrides and precipitation hardening, although there was a

contribution from some other mechanism, most likely interstitial or solid solution hardening or residual stresses. At the highest dose examined, the maximum nitrogen concentration reached approximately 43 at%.

6. RECOMMENDATIONS

There are a number of experiments that might further the understanding of the results obtained in this report. A chemical and microstructural evaluation of the implanted surfaces via x-ray photoelectron spectroscopy and transmission electron microscopy might verify the presence of chromium nitrides and suggest more definitive mechanisms for the improvement in tribological properties. The elevated temperature implantations might also be performed at slightly lower temperatures to determine if the beneficial effects observed in the wear and friction properties at the intermediate doses was a result of softening of the base chromium or due to the broadening of the concentration profiles. It would also be interesting to observe if the hardness increase in the elevated temperature samples is comparable to or better than the room temperature condition. Samples implanted at room temperature might also be annealed after implantation and compared to the elevated temperature samples. This might determine if the diffusion observed in the nitrogen concentration profiles is the result of thermal diffusion alone or the result of effects in the elevated temperature implantation process.

REFERENCES

1. P. D. Townsend, J. C. Kelly, and N. E. W. Hartley, in *Ion Implantation, Sputtering and Their Applications,* (Academic Press, New York, 1976) pp. 1-2.

2. G. Dearnaley, J. H. Freeman, R. S. Nelson, and J. Stephen, in *Ion Implantation,* (North-Holland, Amsterdam, 1973).

3. L. J. Bredell, J. B. Malherbe, *Thin Solid Films*, **228** (1993) p. 267.

4. L. J. Liu, W. Zhou, D. K. Sood, R. Manory, *Materials Research Society Symposium Proceedings*, **279** (1993) p. 469.

5. M. Chen, S. Patu, J. N. Shen, C. X. Shi, *Journal of Materials Research*, **8** (1993) p. 734.

6. S. N. Bunker, A. J. Armini, *Journal of the American Ceramic Society*, **76** (1993) p. 347.

7. G. Dearnaley, *Clinical Materials*, **12** (1993) p. 237.

8. C. J. Sofield, S. Sugden, J. Ing, L. B. Bridwell, Y. Q. Wang, *Vacuum*, **44** (1993) p. 285.

9. S. Murarka and M. Peckerar, in *Electronic Materials: Science and Technology,* (Academic Press, San Diego, 1989) pp. 218-55.

10. J. Mayer and S. Lau, in *Electronic Materials Science: For Integrated Circuits in Si and GaAs,* (Macmillan Publishing, New York, 1990) pp. 227-33.

11. E. W. Thomas, in *Ion Plating and Implantation, Applications to Materials,* ed. by R. F. Hochman (ASM, 1986) p. 7.

12. L. Xie, F. J. Worzala, J. R. Conrad, R. A. Dodd, K. Sridharan, *Materials Science and Engineering*, **A139** (1991) p. 179.

13. S. Lucas, G. Terwagne, M. Piette, F. Bodart, *Nuclear Instruments and Methods in Physics Research*, **B59/60** (1991) p. 925.

14. C. A. Straede, *Nuclear Instruments and Methods in Physics Research*, **B68** (1992) p. 380.

15. J. P. Riviere, J. Delafond, *Surface Engineering*, **9** (1993) p. 59.

16. G. A. Collins, R. Hutchings, J. Tendys, *Materials Science and Engineering*, **A139** (1991) p. 171.

17. B. P. Wood, J. T. Scheuer, M. A. Nastasi, R. H. Olsher, W. A. Reass, I. Henins, D. J. Rej, *Materials Research Society Symposium Proceedings*, **279** (1993) p. 345.

18. J. I. Onate, J. K. Dennis, S. Hamilton, *Metal Finishing*, **87** (1989) p. 25.

19. L. Guzman, L. Ciaghi, F. Giacomozzi, E. Voltolini, A. Peacock, G. Dearnaley, P. Gardner, *Materials Science and Engineering*, **A116** (1989) p. 183.

20. G. Fischer, G. E. Welsch, M. Kim, R. Schieman, *Wear*, **146** (1991) p. 1.

21. M. F. Stroosnijder, J. F. Norton, V. Guttmann, M. J. Bennett, J. H. W. De Wit, *Materials Science and Engineering*, **A116** (1989) p. 103.

22. D. C. Kothari, L. Guzman, S. Girardi, A. Tomasi, S. Gialanella, P. M. Raole, P. D. Prabhawalkar, *Materials Science and Engineering*, **A116** (1989) p. 135.

23. R. C. Lobb, M. J. Bennett, *Oxidation of Metals*, **35** (1991) p. 35.

24. G. K. Hubler, in *Ion Implantation for Materials Processing*, ed. by F. A. Smidt (Noyes Data Corporation, New Jersey, 1983) p. 55.

25. E. H. Lee, L. K. Mansur, *Journal of Materials Research*, **4** (1989) p. 1371.

26. *Metals Handbook*, Volume 5 (ASM, Metals Park, OH, 1982) pp. 170, 183.

27. G. F. Vander Voort, in *Metallography, Principles and Practice*, (McGraw-Hill, New York, 1984) pp. 374-382.

28. H. Ferber, C. K. Mount, G. B. Hoflund, S. Hoshino, *Thin Solid Films*, **203** (1991) p. 121.

29. K. Terashima, T. Minegishi, M. Iwaki, K. Kawashima, *Materials Science and Engineering*, **90** (1987) p. 229.

30. R. Hutchings, *Materials Science and Engineering*, **69** (1985) p. 129.

31. W. C. Oliver, R. Hutchings, J. B. Pethica, *Metallurgical Transactions A*, **15A** (1984) p. 2221.

32. H. Ferber, C. K. Mount, G. B. Hoflund, S. Hoshino, *Nuclear Instruments and Methods in Physics Research*, **B59/60** (1991) p. 957.

33. H. Ferber, C. K. Mount, G. B. Hoflund, S. Hoshino, *Surface and Interface Analysis*, **16** (1990) p. 488.

34. E. Hechtl, J. Bohdansky, J. Roth, *Journal of Nuclear Materials*, **103 & 104** (1981) p. 333.

35. W. O. Hofer, H. L. Bay, P. J. Martin, *Journal of Nuclear Materials*, **76 & 77** (1978) p. 156.

36. D. E. Harrision, Jr., *Radiation Effects*, **70** (1983) p. 1.

TECHNICAL REPORT INTERNAL DISTRIBUTION LIST

	NO. OF COPIES
CHIEF, DEVELOPMENT ENGINEERING DIVISION	
ATTN: AMSTA-AR-CCB-DA	1
-DB	1
-DC	1
-DD	1
-DE	1
CHIEF, ENGINEERING DIVISION	
ATTN: AMSTA-AR-CCB-E	1
-EA	1
-EB	1
-EC	
CHIEF, TECHNOLOGY DIVISION	
ATTN: AMSTA-AR-CCB-T	2
-TA	1
-TB	1
-TC	1
TECHNICAL LIBRARY	
ATTN: AMSTA-AR-CCB-O	5
TECHNICAL PUBLICATIONS & EDITING SECTION	
ATTN: AMSTA-AR-CCB-O	3
OPERATIONS DIRECTORATE	
ATTN: SMCWV-ODP-P	1
DIRECTOR, PROCUREMENT & CONTRACTING DIRECTORATE	
ATTN: SMCWV-PP	1
DIRECTOR, PRODUCT ASSURANCE & TEST DIRECTORATE	
ATTN: SMCWV-QA	1

NOTE: PLEASE NOTIFY DIRECTOR, BENÉT LABORATORIES, ATTN: AMSTA-AR-CCB-O OF ADDRESS CHANGES.

TECHNICAL REPORT EXTERNAL DISTRIBUTION LIST

	NO. OF COPIES
ASST SEC OF THE ARMY RESEARCH AND DEVELOPMENT ATTN: DEPT FOR SCI AND TECH THE PENTAGON WASHINGTON, D.C. 20310-0103	1
ADMINISTRATOR DEFENSE TECHNICAL INFO CENTER ATTN: DTIC-OCP (ACQUISITION GROUP) BLDG. 5, CAMERON STATION ALEXANDRIA, VA 22304-6145	2
COMMANDER U.S. ARMY ARDEC ATTN: SMCAR-AEE	1
SMCAR-AES, BLDG. 321	1
SMCAR-AET-O, BLDG. 351N	1
SMCAR-FSA	1
SMCAR-FSM-E	1
SMCAR-FSS-D, BLDG. 94	1
SMCAR-IMI-I, (STINFO) BLDG. 59 PICATINNY ARSENAL, NJ 07806-5000	2
DIRECTOR U.S. ARMY RESEARCH LABORATORY ATTN: AMSRL-DD-T, BLDG. 305 ABERDEEN PROVING GROUND, MD 21005-5066	1
DIRECTOR U.S. ARMY RESEARCH LABORATORY ATTN: AMSRL-WT-PD (DR. B. BURNS) ABERDEEN PROVING GROUND, MD 21005-5066	1
DIRECTOR U.S. MATERIEL SYSTEMS ANALYSIS ACTV ATTN: AMXSY-MP ABERDEEN PROVING GROUND, MD 21005-5071	1
COMMANDER ROCK ISLAND ARSENAL ATTN: SMCRI-ENM ROCK ISLAND, IL 61299-5000	1
MIAC/CINDAS PURDUE UNIVERSITY. P.O. BOX 2634 WEST LAFAYETTE, IN 47906	1
COMMANDER U.S. ARMY TANK-AUTMV R&D COMMAND ATTN: AMSTA-DDL (TECH LIBRARY) WARREN, MI 48397-5000	1
COMMANDER U.S. MILITARY ACADEMY ATTN: DEPARTMENT OF MECHANICS WEST POINT, NY 10966-1792	1
U.S. ARMY MISSILE COMMAND REDSTONE SCIENTIFIC INFO CENTER ATTN: DOCUMENTS SECTION, BLDG. 4484 REDSTONE ARSENAL, AL 35898-5241	2
COMMANDER U.S. ARMY FOREIGN SCI & TECH CENTER ATTN: DRXST-SD 220 7TH STREET, N.E. CHARLOTTESVILLE, VA 22901	1
COMMANDER U.S. ARMY LABCOM MATERIALS TECHNOLOGY LABORATORY ATTN: SLCMT-IML (TECH LIBRARY) WATERTOWN, MA 02172-0001	2
COMMANDER U.S. ARMY LABCOM, ISA ATTN: SLCIS-IM-TL 2800 POWER MILL ROAD ADELPHI, MD 20783-1145	1

NOTE: PLEASE NOTIFY COMMANDER, ARMAMENT RESEARCH, DEVELOPMENT, AND ENGINEERING CENTER, BENÉT LABORATORIES, CCAC, U.S. ARMY TANK-AUTOMOTIVE AND ARMAMENTS COMMAND, AMSTA-AR-CCB-O, WATERVLIET, NY 12189-4050 OF ADDRESS CHANGES.

TECHNICAL REPORT EXTERNAL DISTRIBUTION LIST (CONT'D)

	NO. OF COPIES
COMMANDER U.S. ARMY RESEARCH OFFICE ATTN: CHIEF, IPO P.O. BOX 12211 RESEARCH TRIANGLE PARK, NC 27709-2211	1
DIRECTOR U.S. NAVAL RESEARCH LABORATORY ATTN: MATERIALS SCI & TECH DIV CODE 26-27 (DOC LIBRARY) WASHINGTON, D.C. 20375	1 1
WRIGHT LABORATORY ARMAMENT DIRECTORATE ATTN: WL/MNM EGLIN AFB, FL 32542-6810	1
WRIGHT LABORATORY ARMAMENT DIRECTORATE ATTN: WL/MNMF EGLIN AFB, FL 32542-6810	1

NOTE: PLEASE NOTIFY COMMANDER, ARMAMENT RESEARCH, DEVELOPMENT, AND ENGINEERING CENTER, BENÉT LABORATORIES, CCAC, U.S. ARMY TANK-AUTOMOTIVE AND ARMAMENTS COMMAND, AMSTA-AR-CCB-O, WATERVLIET, NY 12189-4050 OF ADDRESS CHANGES.